Design and Application of Nano Structure of Solid Catalysts

固体触媒のナノ構造設計と応用

Peipei Zhang

張培培

Supervisor: Prof. Noritatsu Tsubaki

Tsubaki Laboratory

Graduate School of Science and Engineering for Education

University of Toyama

Preface

The utilization of fossil fuel resource, including coal, petroleum and nature gas, has promoted the high speed development of economy and society since the beginning of the industrial revolution. However, excessive consumption of fossil fuel has caused serious environmental problems and the depletion of energy reserves, making abundant researchers to consider the development and employment of renewable and cleaner energy as substitutes for fossil fuels. Biomass is a kind of renewable source of energy, which can be derived from the green plants, perennial grasses, forestry and other plant residues, as well as organic wastes. Converting biomass to produce clean energy, such as hydrogen, syngas, hydrocarbons and other fuels, is one of the most promising option to use renewable energy sources and to decrease the fossil fuel dependence.

Syngas ($CO+H_2$), a type of non-petroleum resource, can be produced from biomass, natural gas and coal. It is an essential platform to transform the lower carbon resource into high value-added products, such as dimethyl ether (DME), light olefins, liquefied petroleum gas (LPG), diesel, even aromatics. Among the process of syngas conversion to hydrocarbons, there are two primarily catalytic approaches in current situation: Fischer-Tropsch synthesis (FTS) and syngas-methanol-hydrocarbons synthesis. Therefore, producing of high value-added chemicals and fuels from syngas has been intensively explored owing to its academic and industrial value.

As we all known, catalyst design is a vital factor in enhancing the catalytic efficiency of catalysis reaction. Moreover, catalyst with unique structure exhibit unexpected performance in catalysis application. As typical representatives, bimodal or core-shell (zeolite capsule structure) structure have attracted wide attention due to their enhanced mass transfer efficiency and specific selectivity to target products. Therefore, in this thesis, we mainly concentrate on the design and application of high performance catalysts with special structure for production of hydrogen from biomass and conversion

of syngas into valuable chemicals: (1) the Ni/ZrO_2-SiO_2-B bimodal pore catalyst for enhanced hydrogen production by steam reforming of vegetable oil (Chapter 1); (2) the Pd/SiO_2-SZ zeolite capsule catalyst for direct synthesis LPG from syngas (Chapter 2); (3) the Cr/Zn-Zn/Z5@S1 hybrid catalyst with Zn/Z5@S1 core-shell structure zeolite for one-pass conversion of syngas to para-xylene (Chapter 3).

In chapter 1, a new Ni/ZrO_2-SiO_2-B bimodal catalyst with specific bimodal structure was developed and applied for hydrogen production from steam reforming of vegetable oil. The bimodal (ZrO_2-SiO_2-B) support was first successfully fabricated by self-assembly of nanosized ZrO_2 inside pores of a commercial silica gel Q-30. For comparison, a unimodal (ZrO_2-SiO_2-U) support was prepared by impregnation of Q-30 with zirconium nitrate. Ni supported bimodal and unimodal ZrO_2-SiO_2, and pristine SiO_2 (Q-30 and Q-3) catalysts were comparatively studied in steam reforming of vegetable oil to hydrogen. Among all catalyst studied bimodal Ni/ZrO_2-SiO_2-B catalyst exhibited highest oil conversion and H_2 formation rate with good stability due to the improved Ni dispersion, enhanced Ni-support interaction, as well as facilitated diffusion of reactant and products, benefiting from bimodal structure and promotional effect of ZrO_2.

In chapter 2, we employed the prepared Pd/SiO_2-SZ zeolite capsule catalyst for the direct synthesis of LPG from syngas. The millimeter-sized zeolite capsule catalyst (Pd/SiO_2-SZ) with a core-shell structure was prepared by a developed dual-layer crystal growth method: coating Silicalite-1 and H-ZSM-5 zeolite orderly as double shells encapsulating the Pd/SiO_2 core catalyst. In the reaction, the zeolite capsule catalyst showed excellent LPG selectivity than the single core catalyst of Pd/SiO_2 and the physical mixture catalyst prepared by a simply mixing core and shell catalysts.

In chapter 3, we presented a promising hybrid catalyst, named Cr/Zn-Zn/Z5@S1, to effectively realize one-pass conversion of syngas to para-xylene. This hybrid catalyst

exhibited enhanced activity on syngas conversion, good stability on catalyst lifetime and considerable selectivity of para-xylene. The characterization and catalytic performance evaluation revealed that the well-designed core-shell Zn/Z5@S1 zeolite, as a vital part of this Cr/Zn-Zn/Z5@S1 hybrid catalyst, substantially contributed its extreme performance for para-xylene one-pass precise synthesis from syngas. The concerted combination of two components in this hybrid catalyst can effectively depress the formation of unwanted by-products and facilitate the oriented synthesis of para-xylene from syngas with unprecedented efficiency at the same time.

Herein, three types of catalysts with special structures were successfully designed, synthesized and applied to transform the biomass/syngas resource into high-value-added chemicals. The physical-chemical properties and catalytic performances of these efficient catalysts were also studied.

Contents

Chapter 1

Enhanced Hydrogen Production from Steam Reforming of Vegetable Oil over Bimodal ZrO_2-SiO_2 Supported Ni Catalyst

A ZrO_2-SiO_2 bimodal was fabricated by self-assembly of nanosized ZrO_2 inside silica Q-30, and Ni supported bimodal catalyst was applied in hydrogen production from steam reforming of vegetable oil.

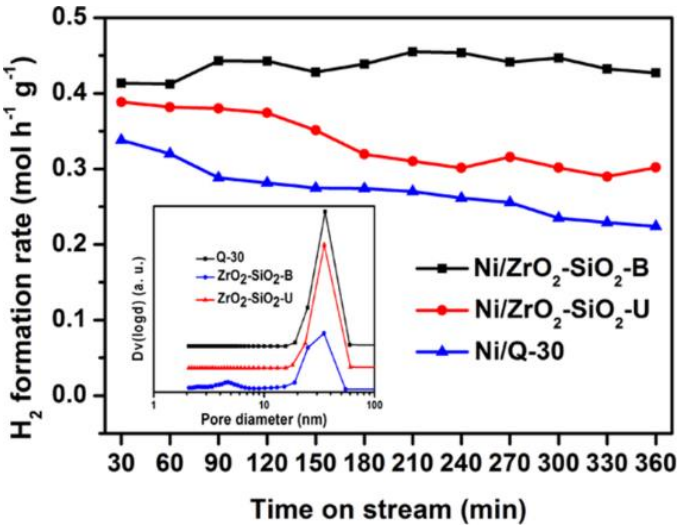

Abstract

Bimodal (ZrO_2-SiO_2-B) support was successfully fabricated by self-assembly of nanosized ZrO_2 inside pores of a commercial silica gel Q-30. For comparison, a unimodal (ZrO_2-SiO_2-U) support was prepared by impregnation of Q-30 with zirconium nitrate. Ni supported bimodal and unimodal ZrO_2-SiO_2, and pristine SiO_2 (Q-30 and Q-3) catalysts were comparatively studied in steam reforming of vegetable oil to hydrogen. The support and catalyst were analyzed by various techniques, such as N_2 physisorption, XRD, TPR, H_2 chemisorption and TGA. Characterization results indicated that bimodal support showing increased BET surface area was beneficial for the dispersion of Ni species. TPR result showed that the incorporation of ZrO_2 improved the reducibility of NiO and enhanced the metal-support interaction, simultaneously. Among all catalyst studied bimodal Ni/ZrO_2-SiO_2-B catalyst exhibited highest oil conversion and H_2 formation rate with good stability due to the improved Ni dispersion, enhanced Ni-support interaction, as well as facilitated diffusion of reactant and products, benefiting from bimodal structure and promotional effect of ZrO_2.

Keywords: Bimodal, ZrO_2-SiO_2, H_2 formation, Ni, Vegetable Oil

1.1. Introduction

Hydrogen is an important industrial feedstock for versatile applications. It is widely applied in ammonia, methanol synthesis and petrochemical industry. Apart from these traditional applications, hydrogen has been regarded as a clean energy carrier, used in fuel cell. Fuel cell, which mainly based on hydrogen, generates power with high efficiency and no pollution, because water is the only by-product [1,2]. At present, hydrogen is mainly produced by steam reforming of fossil fuels such as natural gas, coal and naphtha [3,4]. But this process generates large amounts of carbon dioxide, which is a well-known greenhouse gas, causing global warming and climate change. Besides, fossil fuels are non-renewable. For these reasons, it is crucial to produce hydrogen from alternative feedstocks cleanly and renewably [1,5]. Among various feedstocks, biomass has been recognized as a potential renewable resource, as it can make us less dependent on fossil fuels for power or transport and offer a carbon dioxide neutral energy supply [6]. Several routes have been explored for producing hydrogen from biomass, such as gasification [7], fast pyrolysis of biomass followed by steam reforming of the obtained bio-oil [2,8].

Vegetable oils and fats have been used as an alternative feedstock for fuel and chemicals production, attracting great interest during the last decades [9,10]. It is believed that vegetable oils is a potential candidate for hydrogen production, as their oxygen content is low and hydrogen yield is high, and steam reforming was an efficient way of producing hydrogen from vegetable oil [11,12]. The general steam reforming of vegetable oil is given by Eq. (1-1) [13]. Carbon monoxide could be further converted to carbon dioxide and hydrogen via water gas shift (WGS) reaction (Eq. (1-2)). Besides, side reactions, such as cracking (Eq. (1-3)) and methanation (Eq. (1-4)) etc. are usually involved.

$$C_nH_mO_k + (n-k)H_2O \leftrightarrow nCO + (n+\frac{m}{2}-k)H_2 \quad \Delta H^{\Theta}_{298K} > 0 \qquad (1\text{-}1)$$

$$CO + H_2O \leftrightarrow H_2 + CO_2 \quad \Delta H^{\Theta}_{298K} = -41.2 KJ/mol \qquad (1\text{-}2)$$

$$C_nH_mO_k \leftrightarrow (\frac{n}{2}-k)C + (\frac{3m}{8}-\frac{n}{2})H_2 + \frac{n}{4}CH_4 + \frac{1}{4}C_nH_m + kCO \quad \Delta H^{\Theta}_{298K} > 0 \qquad (1\text{-}3)$$

$$CO + 3H_2 \leftrightarrow CH_4 + H_2O \quad \Delta H^{\Theta}_{298K} = -206 KJ/mol \qquad (1\text{-}4)$$

Nickel-based catalyst has been proved to be a promising catalyst for reforming reactions [11,14]. Many reforming catalysts employ appropriate supports to disperse active metal or metal compounds. Metal oxides with large surface and high thermal stability, such as silica or alumina are widely used as supports for reforming reactions. The support has a profound effect on the physico-chemical properties of catalyst and the corresponding catalytic performance. Generally, for inorganic solids with conventional morphologies, there is reverse relationship between surface area and pore size [15]. A support with large surface area contains a large portion of small size pores. The use of large surface support will lead to small metal particle size with high metal dispersion, but high inter-pellet diffusion resistance. The application of low surface support can achieve high metal reducibility, fast diffusion of reactants and products, but result in low metal dispersion and large metal particle size. Moreover, the role of support is not limited to maintain the catalytically active phase at a highly dispersed state, and it may also contribute to catalytic activity due to the chemical effect or interaction between the active phase and the support phase.

An alternative way to improve catalytic performance of reforming catalyst is the addition of promoters. Zirconia has been presently employed as either a promoter or a support for Ni and Pt active components in many reforming reactions, due to its redox behaviour, reducibility, surface acidity and high thermal stability [16-18]. Besides, the method of catalyst preparation can also be used to adjust catalytic performance [19].

In the present study, we firstly reported bimodal ZrO_2-SiO_2 supported Ni catalyst for hydrogen production from steam reforming of vegetable oil. For comparison, a

unimodal ZrO_2-SiO_2 was also prepared. The catalytic performance of the bimodal ZrO_2-SiO_2, unimodal ZrO_2-SiO_2 and pristine SiO_2 supported Ni catalysts was compared. The effects of pore structure of supports and the promotional effect of ZrO_2 addition were investigated in detail by employing multiple physicochemical characterizations such as, XRD, N_2 physisorption, TPR, H_2-chemisorption and TGA.

1.2. Experimental section

1.2.1 Preparation of Ni/SiO_2 and Ni/ZrO_2-SiO_2 catalysts

Bimodal ZrO_2-SiO_2 support (ZrO_2-SiO_2-B) was prepared by incipient-wetness impregnation of silica gel Q-30 with ZrO_2 sol. In a typical synthesis, 2 g of Q-30 was placed in a crucible. Then, 2.6 ml of aqueous solution containing 3.0 g ZrO_2 sol was dropsized into the crucible under stirring with a glass rod. The impregnation was facilitated with aid of ultrosolication. After the impregnation, the support was directly calcined in air at 500 ^oC for 2 h to achieve bimodal pore structure since the presence of water vapor was beneficial for the aggregation of nanosized ZrO_2 particles, forming mesopores [20]. For comparison, unimodal ZrO_2-SiO_2 support (ZrO_2-SiO_2-U) was prepared by the same process as that of bimodal support, excepting that $ZrO(NO_3)_2 \cdot 2H_2O$ was used as Zr precursor instead of ZrO_2 sol. The impregnated sample was dried at 120 ^oC overnight, followed by calcining at 500 ^oC for 2 h. The loading of ZrO_2 was 20 wt% unless otherwise stated. 5 wt% Ni supported catalysts were prepared by incipient-wetness impregnation method. Typically, 2 g of support was impregnated with required amount of aqueous solution containing 0.11 g nickel nitrate hexahydrate, followed by drying at 120 ^oC for 12 h and finally calcined at 600 ^oC for 2 h.

1.2.2 Characterization

N_2 physisorption experiment was performed at -196 ^oC using Quantachrome Autosorb-1B apparatus. The sample was outgassed at 200 ^oC for 2 h before each test.

The BET surface area was calculated using the multiple BET method, and the pore size was measured by the BJH method using desorption branch of the nitrogen isotherms.

Powder X-ray diffraction (XRD) patterns of the studied catalysts were obtained with a Rigaku RINT2000 diffractometer using Cu Kα radiation. The NiO particle size was calculated by Scherrer equation: $L = K\lambda / D(2\theta)\cos(\theta_0)$, where L was the crystalline size, K was a constant (K=0.9-1.1), λ was wavelength of X-ray (Cu Kα=0.154 nm), and D was the width of the peak at half height.

Temperature programmed reduction (TPR) experiment was performed on a BELCAT-B (BEL JAPAN) catalyst analyser. In a typical test, 30 mg catalyst was temperature-programmed reduced by a 5 vol. % H_2/Ar flow (50 ml/min) from 50 ^oC to 800 ^oC with a ramping rate of 10 ^oC/min. Hydrogen consumption was monitored by thermal conductivity detector (TCD). Prior to each measurement, the sample was dried at 150 ^oC for 1 h in an Ar (50 ml/min) atmosphere to remove the impurities and moisture. H_2 chemisorption experiment was performed at 100 ^oC in BELCAT-B (BEL JAPAN) equipment using pulse injection method. The passivated catalyst was in situ reduced at 400 ^oC for 1 h by a 5 vol. % H_2/Ar flow (50 ml/min). After the reduction, the sample was cooled down to 100 ^oC in an Ar flow, and then several H_2 pulses were injected until saturated chemisorption was achieved. The amount of gas adsorbed was determined from the difference in the gas volume of introduced and remained in the sample.

Ni metal dispersion was calculated from adsorbed H_2 volume assuming the adsorption stoichiometry of one hydrogen atom per nickel surface atom (H/Ni=1).

Coke deposition on spent catalyst after steam reforming was analyzed by thermogravimetric (TG) analysis (DTA/TGA-60, Shimadzu). The catalyst was temperature-programmed heated from room temperature to 850 ^oC with a ramp rate of 10 ^oC/min in an air flow (50 ml/min).

1.2.3 Catalytic activity tests

The commercial canola oil was directly used as reactant. The steam reforming reaction was conducted in a continuous flow type fixed-bed stainless steel reactor with an i.d. of 8 mm at atmospheric pressure. The catalyst mixed with quartz sand was loaded in the centre of reactor, and was reduced *in situ* at 400 ^{o}C for 10 h in the flow of pure H_2 (50 ml/min). Then, vegetable oil and H_2O were fed into the reactor by syringe pumps, using N_2 (40 ml/min) as the carrier gas. The vegetable oil and H_2O were vaporized and mixed before entering the reactor. An ice trap was used to recover the unreacted vegetable oil and water. Gaseous products released from the reactor were analysed by two online gas chromatographs (GC). H_2 was analysed by Shimadzu GC-8A equipped with a TCD using an activated carbon column. CO, CO_2 and hydrocarbons were analysed by Shimadzu GC-9A equipped with a flame ionization detector (FID) and a methanator employing a Porapak Q column. Vegetable oil conversion, selectivity of products and yield of H_2 were calculated as follows:

$$\text{Oil conversion (wt\%)} = \frac{\text{Oil}_{\text{feed}} - \text{Oil}_{\text{trap}}}{\text{Oil}_{\text{feed}}} \times 100\% \quad (1\text{-}5)$$

$$\text{P}_\text{i}\ \text{selectivity} = \frac{\text{Amount of P}_\text{i}\ \text{in carbon mole}}{\text{Total amount of products in carbon mole}} \quad (1\text{-}6)$$

$$\text{H}_2\ \text{yield} = \text{Oil conversion} \times \frac{\text{Amount of H}_2\ \text{produced (mol)}}{\text{Total amount of products (mol)}} \quad (1\text{-}7)$$

(P_i represents CO, CO_2, CH_4 and hydrocarbons)

For the definition of hydrogen yield the theoretical amount is the hydrogen produced from the complete steam reforming reaction.

$$\text{H}_2\ \text{yield} = \frac{\text{Moles of hydrogen produced (mol)}}{\text{Theoretical moles of hydrogen (mol)}} \times 100\% \quad (1\text{-}8)$$

1.3. Results and discussion

1.3.1 Catalyst characterization

1.3.1.1 Physicochemical property of SiO_2 and ZrO_2-SiO_2 supports

In the present study, bimodal ZrO_2-SiO_2 was fabricated by introduction of ZrO_2 sol inside of a commercial silica gel Q-30 while a unimodal ZrO_2-SiO_2 support was also

prepared using $ZrO(NO_3)_2 \cdot 2H_2O$ as the precursor of ZrO_2. The porosity of silica and ZrO_2-SiO_2 supports was measured by N_2 physisorption. The pore size distribution of original silica Q-30, ZrO_2-SiO_2-B and ZrO_2-SiO_2-U samples are present in Figure 1.1. It is found that Q-30 show a uniform pore size distribution centered around 35.8 nm. After the impregnation with $ZrO(NO_3)_2 \cdot 2H_2O$, the pore size distribution of ZrO_2-SiO_2-U slightly changed with peak maxima shifted to 35.0 nm. Interestingly, as for the ZrO_2-SiO_2-B sample, distinguished bimodal pore structure after the incorporation of ZrO_2 sols inside silica Q-30 found. The larger pores around 34.8 nm was inherited from pristine silica Q-30, and the smaller pores centred at 4.7 nm was generated by the self-organization of nanosized ZrO_2. The BET surface, pore volume and pore size are summarized in Table 1.1. The BET surface area and pore volume of original silica Q-30 were 122.8 m^2/g and 1.31 ml/g, respectively. The ZrO_2-SiO_2-U sample showed decreased BET surface, pore volume and mean pore size on account of the blocking of pores by Zr species. However, the ZrO_2-SiO_2-B sample exhibited significantly increased BET surface area, which was twice that of original silica Q-30. The enlarged BET surface area was ascribed to smaller pores (4.7 nm), generating from the packing of nanosized ZrO_2 inside pores of silica Q-30. N_2 physisorption results suggested that the pore structure of ZrO_2-SiO_2 was closely related to the precursor of Zr, and the bimodal structure could be obtained when ZrO_2 sol was employed.

1.3.1.2 XRD analysis

The crystalline structure of Ni based catalysts was studied by XRD. The XRD patterns of Ni/SiO_2 and Ni/ZrO_2-SiO_2 catalysts are shown in Figure 1.2. All samples show a broad diffraction peak centered on 2θ of 21.58, which was ascribed to amorphous silica [20]. Besides, several characteristic diffraction peaks of NiO are also observed for all samples. It is should be noted that no ZrO_2 related diffraction peak is found for Zr containing Ni/ZrO_2-SiO_2-U and Ni/ZrO_2-SiO_2-B samples, suggesting formation of nanosized ZrO_2 below the detect limit of XRD or amorphous phase. The

crystalline size of NiO, calculated by Scherrer equation, is presented in Table 1.2. The composition of catalyst determined by energy dispersive X-ray (EDX) analysis is shown in Table 1.2. The Ni/Q-3 showed smallest NiO size (7.0 nm), since the largest BET surface area of Q-3 support. In contrary, the NiO size of Ni/Q-30 was 20.2 nm, much bigger than that of Ni/Q-3, considering the low BET surface area of Q-30 (122.8 m^2/g) support. Ni/ZrO_2-SiO_2-U unimodal catalyst showed decreased NiO particle size (16.5 nm) due to the promotional effect of ZrO_2 [21]. The NiO size of Ni/ZrO_2-SiO_2-B bimodal catalyst was even smaller, which was 14.8 nm. It was suggested that apart from the promotional effect of ZrO_2 modification, the enhanced BET surface area of support provided by bimodal structure contributed to the improved dispersion of Ni species.

1.3.1.3 H_2-TPR analysis

To reveal the interaction between Ni species and the support, TPR experiments were performed. Figure 1.3 shows the TPR profiles of Ni/SiO_2 and Ni/ZrO_2/SiO_2 samples. For Ni/Q-30, a reduction band in the range of 200-420 ^oC with peak maxima centered around 346 ^oC, which could be ascribed to the reduction of bulk NiO interacting weakly with the support [21,22]. Ni/Q-3 showed a broad reduction peak centered around 420 ^oC, indicating stronger interaction with the support since the NiO size of Ni/Q-3 was much smaller than that of Ni/Q-30. Ni/ZrO_2-SiO_2-U sample displayed three reduction bands. The first two bands were attributed to the reduction of NiO with weak interaction with the support. Compared with Ni/Q-30, a broad shoulder was appeared in range of 150-300 ^oC, indicating that the reducibility of NiO was improved after introduction of ZrO_2 [23]. Besides, a high temperature shoulder in the range of 450-580 ^oC was also observed, assigned to the reduction of Ni species strongly interacting with the support [21]. The TPR profile of Ni/ZrO_2-SiO_2-B was similar to that of Ni/ZrO_2-SiO_2-U. However, it is observed that the low-temperature shoulder slightly shifts to lower temperature, and the high-temperature shoulder slightly shifts to higher temperature, suggesting higher reducibility and stronger interaction between NiO

species and the support for bimodal catalyst. The strong metal-support interaction would be beneficial for stabilizing nanosized active Ni sites during the steam reforming reaction.

1.3.1.4 H_2 chemisorption analysis

The chemisorption measurement was performed to determine the dispersion of Ni, and the result is given in Table 1.2. It is revealed that the increasing the BET surface area of the support and incorporating Zr could improve the dispersion of Ni. Thus, Ni/ZrO_2-SiO_2-B bimodal catalyst showed higher Ni dispersion (7.1%) than those of Ni/ZrO_2-SiO_2-U (6.3%) and Ni/Q-30 (4.9%) unimodal catalysts.

1.3.2 Reaction performance of steam reforming of vegetable oil

The catalysts were applied in steam reforming of commercial canola oil. The H_2 formation rate of catalysts is shown in Figure 1.4. Although the NiO size of Ni/Q-3 catalyst was fine (7 nm), the catalyst showed poor catalytic performance. The initial H_2 formation rate of Ni/Q-3 was low, and declined sharply after 2 h of reaction. This was caused by the fact that the pore size of Q-3 was small (around 3 nm), which was not beneficial for the intra-pellet diffusion of the heavy canola oil molecule, resulting poor efficiency of active sites. Besides, the blocking of small pore stimulated side reactions, such as coking, resulted in deactivation. The initial H_2 formation rate of Ni/Q-30 was higher than that of Ni/Q-3, since the catalyst containing larger pores (30 nm), facilitating the transportation of reactants and products. Compared with Ni/Q-30, Ni/ZrO_2-SiO_2-U showed an improved H_2 formation rate due to improved Ni species dispersion and reducibility after Zr incorporation. The activity gradually decreased with time on stream. Of all samples examined, Ni/ZrO_2-SiO_2-B exhibited highest H_2 formation rate without obvious decline after 6 h of reaction. The vegetable oil conversion, H_2 yield and product selectivity of catalysts are summarized in Table 1.3. It was found that bimodal catalyst exhibited highest oil conversion (92.5%) and H_2

selectivity (60.2%). On the one hand, the enlarged BET surface area provided by newly born small pores of bimodal catalyst, leading to improved Ni dispersion. On the other hand, the retained large pores of bimodal catalyst accelerated the transportation of oil and products, improving the efficiency of catalyst. Besides, incorporation of ZrO_2 promoted the dispersion of Ni species and enhanced the interaction between Ni species and the support. All these factors contributed to the high catalytic activity and stability of bimodal catalyst.

The effect of reaction temperature on oil conversion and H_2 yield of Ni/ZrO_2-SiO_2-B bimodal catalyst was investigated and shown in Figure 1.5. The oil conversion at 500 ^oC was 67.5%. As temperature elevated, the oil conversion significantly increased and reached 100% at 650 ^oC. Steam reforming of vegetable oil was strongly endothermic. Thus, high temperature was desirable for the conversion of vegetable oil from a thermodynamic point of view. H_2 yield was also increased with temperature increased to 600 ^oC. However, no obvious change of H_2 yield was found when further increasing the temperature. Side reactions, such as thermal cracking was usually unavoidable during the steam reforming of vegetable oil [11]. In fact, in this work, blank reaction without catalyst was also performed. The result suggested that around 15% of oil was converted with negligible amount of H_2 detected. So, at high temperature, thermal cracking dominated, lowering the yield of H_2. Consequently, 600 ^oC was selected as reaction temperature to study the steam reforming of vegetable oils in order to achieve considerable oil conversion and H_2 yield, and suppress the cracking reactions.

The influence of steam-to-carbon (S/C) ratio on catalytic performance of Ni/Q-30 and Ni/ZrO_2-SiO_2-B bimodal catalyst was studied and shown in Figure 1.6. When the S/C ratio decreased from 5 to 3, both oil conversion and H_2 yield declined apparently for Ni/Q-30. But, in the case of Ni/ZrO_2-SiO_2-B bimodal catalyst, these values slightly changed, indicating superior catalytic performance of bimodal catalyst. Practically,

lower S/C ratio meant less energy required for evaporating the water. Therefore, the reforming reaction was conducted at S/C ratio of 3.

The catalytic performance of bimodal catalyst was further compared with commercial reforming catalyst RUA (Al:Fe:Ru=96.5:0.5:3.0) and FCR (Al:Ni=75:25). Figure 1.7 shows H_2 formation rates of three catalysts. Obviously, bimodal catalyst exhibited much higher H_2 formation rate than that of RUA or FCR, suggesting the advantage of this kind of bimodal catalyst.

1.3.3 Characterization of spent Ni based catalysts

The post-reaction catalyst was analyzed by TG to detect the possible coke deposition after reforming. Figure 1.8 shows the TG curves of spent Ni/Q-30 and Ni/ZrO_2-SiO_2-B bimodal catalyst. Both catalyst displayed two-stage weight loss behavior. The first mass loss in range of 150-400 ^oC was due to oxidation of activated amorphous carbon, and the second weight loss in 450-600 ^oC range could be ascribed to the removal of graphitized and more inert carbon [22,24]. The total mass loss of bimodal and Ni/Q-30 catalyst was 23.0 and 40.3%, respectively. It can be seen that both the total amount of carbon and graphitized carbon was suppressed over bimodal catalyst. Thus, bimodal catalyst exhibited excellent catalytic activity and stability.

XRD measurement of spent bimodal catalyst was further performed to investigate any change of catalyst. As shown in Figure 1.9, the spent bimodal catalyst exhibited similar XRD profile to that of reduced sample, showing characteristic diffraction peaks of Ni and amorphous SiO_2. The Ni size (calculated by Scherrer equation) of reduced and spent samples were 15.3 and 16.5 nm, respectively, suggesting that the bimodal catalyst was quite stable, and no sintering of Ni was observed. The porosity of spent bimodal catalyst was also investigated by N_2 physisorption. As shown in Figure 1.10, the bimodal porous structure of Ni/ZrO_2-SiO_2-B was mainly retained after reaction in spite of some shrinkage of large pores, indicating superior stability of bimodal catalyst. The characterization results indicated that the bimodal catalyst was quite stable free of

coking, sintering and corrupting of bimodal porous structure, which was in good agreement to its superior catalytic performance for hydrogen production from steam reforming of vegetable oil.

1.4. Conclusions

A bimodal ZrO_2-SiO_2-B support was successfully synthesized by introducing ZrO_2 sol precursors inside pores of a commercial silica gel Q-30 followed by calcination. While a unimodal ZrO_2-SiO_2-U support was obtained when using $ZrO(NO_3)_2 \cdot 2H_2O$ as the precursor. Characterization results indicated that bimodal ZrO_2-SiO_2-B support showing increased BET surface area, compared with unimodal ZrO_2-SiO_2-U support and pristine Q-30 due to the porosity provided by self-organization of ZrO_2 nanoparticles inside Q-30. The increased BET surface led to smaller NiO size (14.8 nm) and higher of Ni dispersion (7.1) than its opponents. TPR result showed that the incorporation of ZrO_2 improved the reducibility of NiO and enhanced the metal-support interaction, simultaneously. Bimodal Ni/ZrO_2-SiO_2-B, unimodal Ni/ZrO_2-SiO_2-U and pristine SiO_2 (Q-30 and Q-3) catalysts were comparatively studied in steam reforming of vegetable oil. Among all catalyst studied bimodal Ni/ZrO_2-SiO_2-B catalyst exhibited highest oil conversion and H_2 formation rate. Analysis of spent catalyst revealed that the bimodal catalyst was quite stable without sintering or damage of bimodal pore structure. It was inferred that the improved Ni dispersion, enhanced Ni-support interaction, as well as facilitated diffusion of reactant and products from bimodal structure, and promotional effect of ZrO_2 contributed to the superior catalytic performance of bimodal catalyst.

References

[1] M. Ni, D. Leung, M. Leung, Int. J. Hydrogen Energy, 2007, 32, 3238-3247.

[2] D. Wang, S. Czernik, D. Montané, M. Mann, E. Chornet, Ind. Eng. Chem. Res., 1997, 36, 1507-1518.

[3] X. Hu, G. Lu, J. Mol. Catal. A, 2007, 261, 43-48.

[4] M. Pena, J. Gomez, J. Fierro, Appl. Catal. A, 1996, 144, 7-57.

[5] A. Basagiannis, X. Verykios, Int. J. Hydrogen Energy, 2007, 32, 3343-3355.

[6] B. Zhang, X. Tang, Y. Li, Y. Xu, W. Shen, Int. J. Hydrogen Energy, 2007, 32, 2367-2373.

[7] W. Hauserman, Int. J. Hydrogen Energy, 1994, 19, 413-419.

[8] M. Marquevich, S. Czernik, E. Chornet, D. Montane, Energy & Fuels, 1999, 13, 1160-1166.

[9] F. Karaosmanoglu, K. Cigizoglu, M. Tuter, S. Ertekin, Energy & Fuels, 1996, 10, 890-895.

[10] S. Katikaneni, J. Adjaye, N. Bakhshi, Energy & Fuels, 1995, 9, 599-609.

[11] M. Marquevich, X. Farriol, F. Medina, D. Montané, Ind. Eng. Chem. Res., 2001, 40, 4757-4766.

[12] M. Marquevich, F. Medina, D. Montané, Catal. Comm., 2001, 2, 119-124.

[13] G. Nahar, V. Dupont, M. Twigg, E. Dvininov, App. Catal. B, 2015, 168-169, 228-242

[14] M. Marquevich, R. Coll, D. Montané, Ind. Eng. Chem. Res., 2000, 39, 2140-2147.

[15] A. Martínez, G. Prieto, J. Rollán, J. Catal., 2009, 263, 292-305.

[16] S. Therdthianwong, Int. J. Hydrogen Energy, 2008, 33, 991-999.

[17] S. Ozkara-Aydinoglu, A. Aksoylu, Catal. Comm., 2010, 11, 1165-1170.

[18] J. Wei, B. Xu, J. Li, Z. Cheng, Q. Zhu, Appl. Catal. A, 2000, 196, L167-L172.

[19] X. Verykios, Int. J. Hydrogen Energy, 2003, 28, 1045-1063.

[20] K. Tao, Q. Ma, N. Tsubaki, S. Zhou, L. Han, J. Mol. Catal. A, 2016, 416, 39-46.

[21] Wang Y, Wu R, Zhao Y, Catal. Today, 2010, 158, 470-474.

[22] K. Tao, S. Zhou, Q. Zhang, C. Kong, Q. Ma, N. Tsubaki, L. Chen, RSC Advances, 2013, 3, 22285-22294.

[23] P. Zhu, Q. Chen, Y. Yoneyama, N. Tsubaki, RSC Advances, 2014, 4, 64617-64624.

[24] Z. Zhang, X. Verykios, Catal. Today, 1994, 21, 589-595.

Table 1.1 Textural properties of pristine silica and ZrO_2-SiO_2 supports.

Supports	S_{BET} (m^2/g)	Pore volume (ml/g)	Pore diameter (nm)
Q-3(SiO_2)	546.0	3.00	3.0
Q-30 (SiO_2)	122.8	1.31	35.8
ZrO_2-SiO_2-U	114.6	0.80	35.0
ZrO_2-SiO_2-B	265.8	0.88	4.7, 34.8

Table 1.2 Physico-chemical property of Ni based catalysts.

Catalysts	NiO particle size (nm)[a]	Ni dispersion (%)[b]	Elemental analysis (%)[c]	
			Ni	Zr
Ni/Q-3	7.0	13.5	4.5	-
Ni/Q-30	20.2	4.9	4.8	-
Ni/ZrO_2-SiO_2-U	16.5	6.3	4.4	13.1
Ni/ZrO_2-SiO_2-B	14.8	7.1	4.7	12.7

[a] NiO particle size calculated from XRD patterns of calcined catalysts. [b] Ni dispersion determined from H_2 chemisorption. [c] Elemental analysis was performed by EDX (presented in weight percent).

Table 1.3 Catalytic performance of Ni based catalysts.

Catalysts	Vegetable oil Conv. (%)[a]	H_2 yield (%)[a]	Selectivity (%)				
			CO	CH_4	CO_2	C_2	C_{3+}
Ni/Q-3	35.8	1.4	3.0	3.4	1.6	21.1	70.9
Ni/Q-30	50.8	34.6	11.4	2.5	34.5	8.0	43.6
Ni/ZrO_2-SiO_2-U	82.5	50.8	11.5	2.4	35.5	4.7	45.8
Ni/ZrO_2-SiO_2-B	92.5	60.2	16.5	3.1	31.6	8.2	40.6

[a]data collected after 3.0 hours of reaction

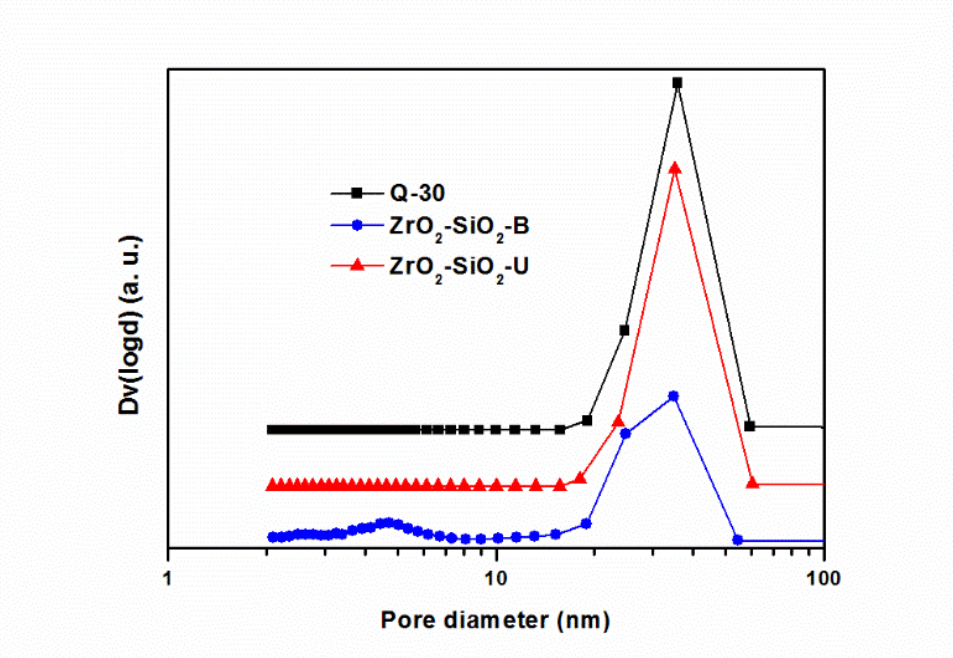

Figure 1.1 Pore size distributions of SiO_2 and ZrO_2-SiO_2 supports.

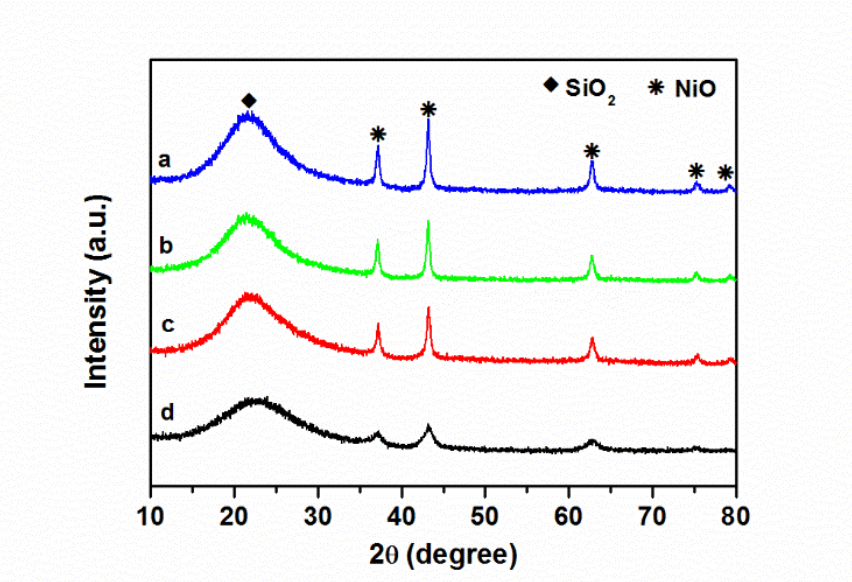

Figure 1.2 XRD patterns of calcined Ni based catalysts: (a) Ni/Q-30, (b) Ni/ZrO_2-SiO_2-U, (c) Ni/ZrO_2-SiO_2-B, and (d) Ni/Q-3.

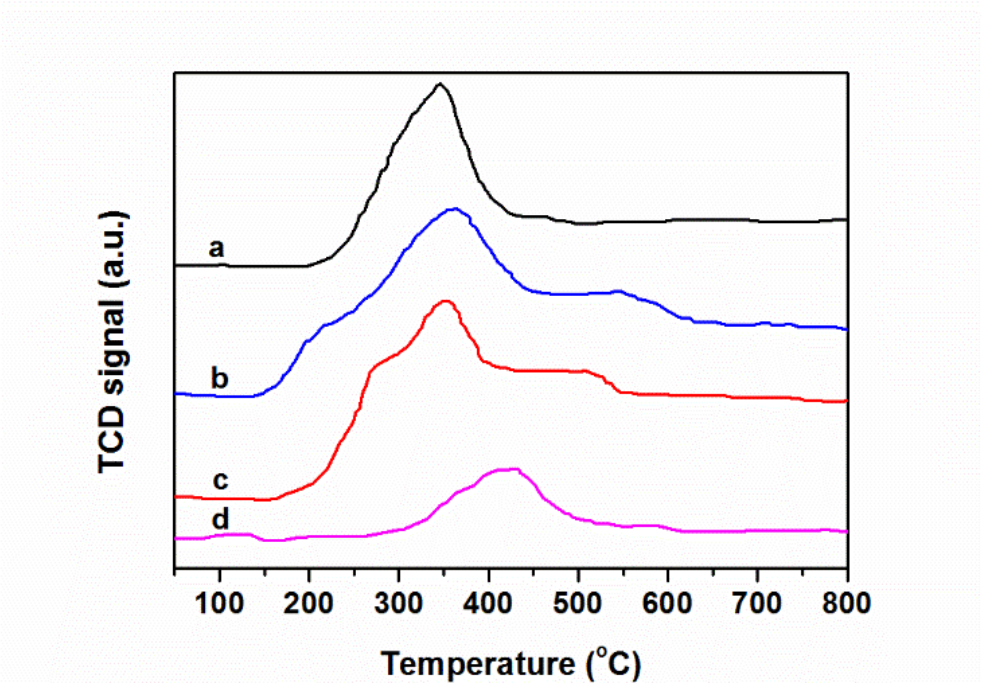

Figure 1.3 TPR profiles of calcined Ni based catalysts: (a) Ni/Q-30, (b) Ni/ZrO_2-SiO_2-B, (c) Ni/ZrO_2-SiO_2-U, and (d) Ni/Q-3.

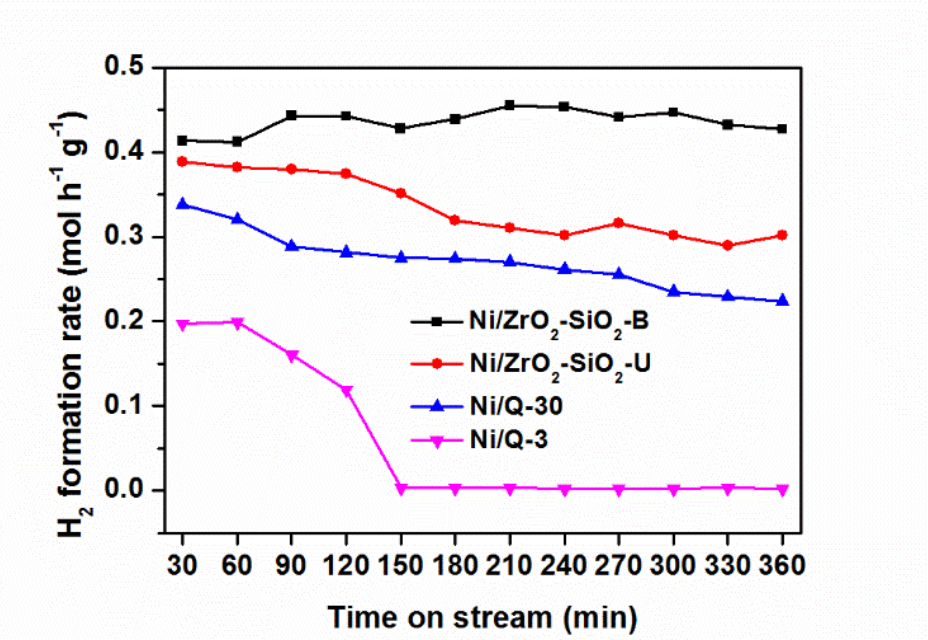

Figure 1.4 H_2 formation rate of various catalysts. Reaction condition: catalyst weight = 0.1 g; T=600 °C; P=0.1 MPa; S/C=3; LHSV=5.4 h^{-1}.

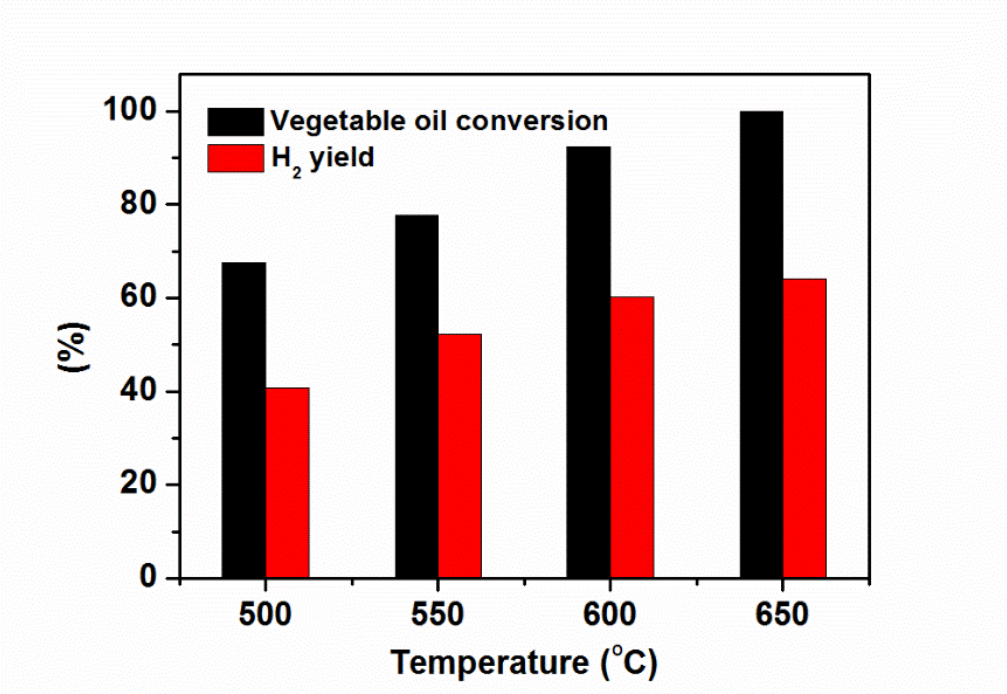

Figure 1.5 The effect of reaction temperature on catalytic performance of Ni/ZrO_2-SiO_2-B bimodal catalyst. Reaction condition: catalyst weight=0.1 g; P=0.1 MPa; S/C=3; LHSV=5.4 h^{-1}.

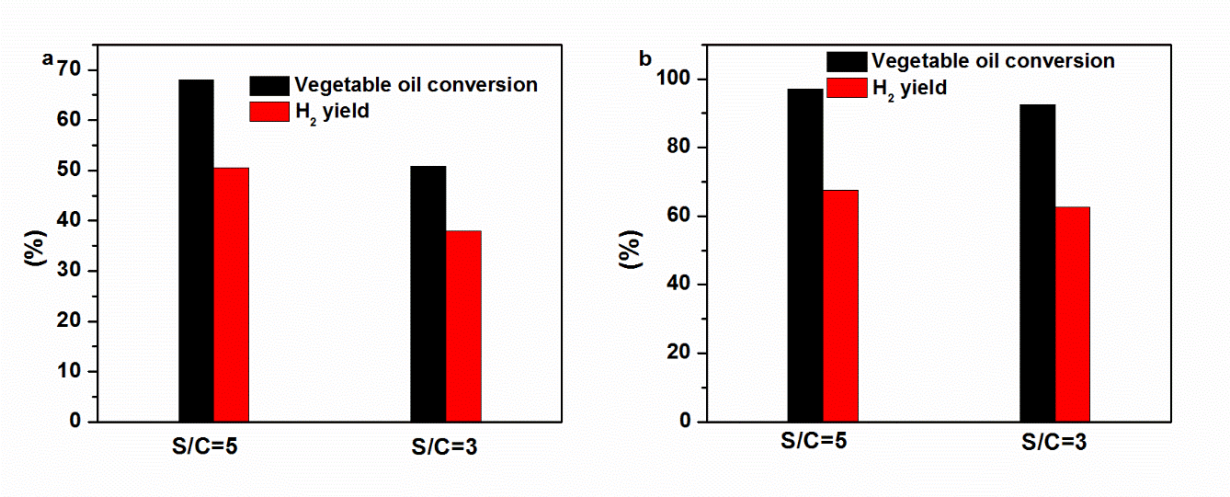

Figure 1.6 The effect of S/C ratio on catalytic performance of Ni/Q-30 (a) and Ni/ZrO_2-SiO_2-B (b) bimodal catalyst. Reaction condition: catalyst weight=0.1 g; T=600 °C; P=0.1 MPa; LHSV=5.4 h^{-1}.

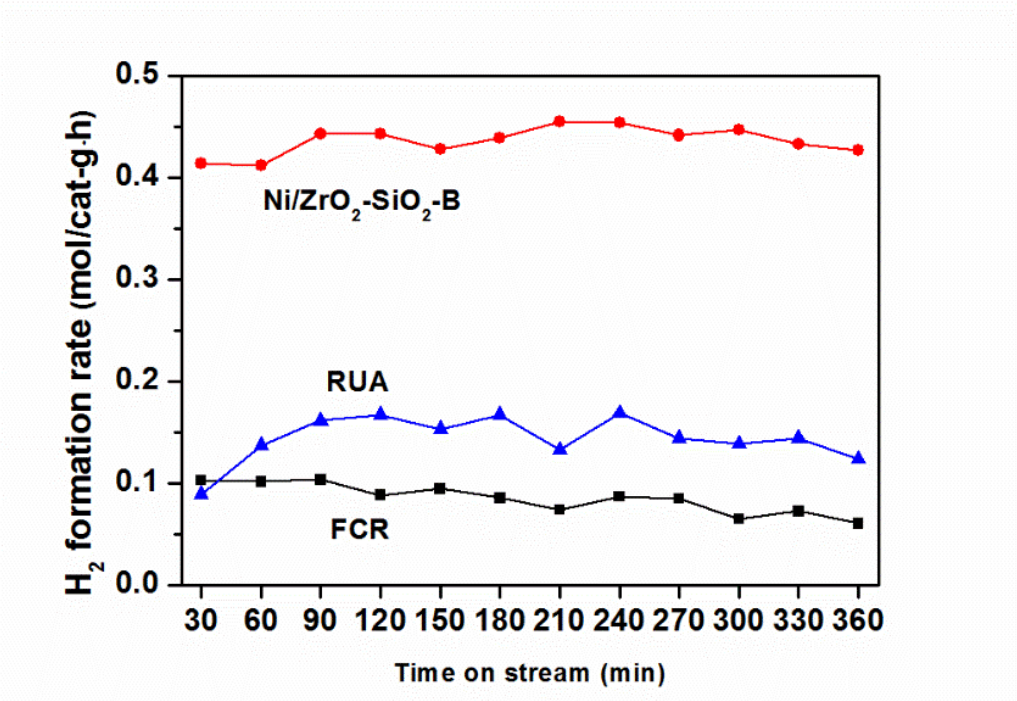

Figure 1.7 H_2 formation rate of commercial RUA and FCR, and Ni/ZrO_2-SiO_2-B bimodal catalyst. Reaction condition: catalyst weight=0.1 g; T=600 °C; P=0.1 MPa; S/C=3; LHSV=5.4 h^{-1}.

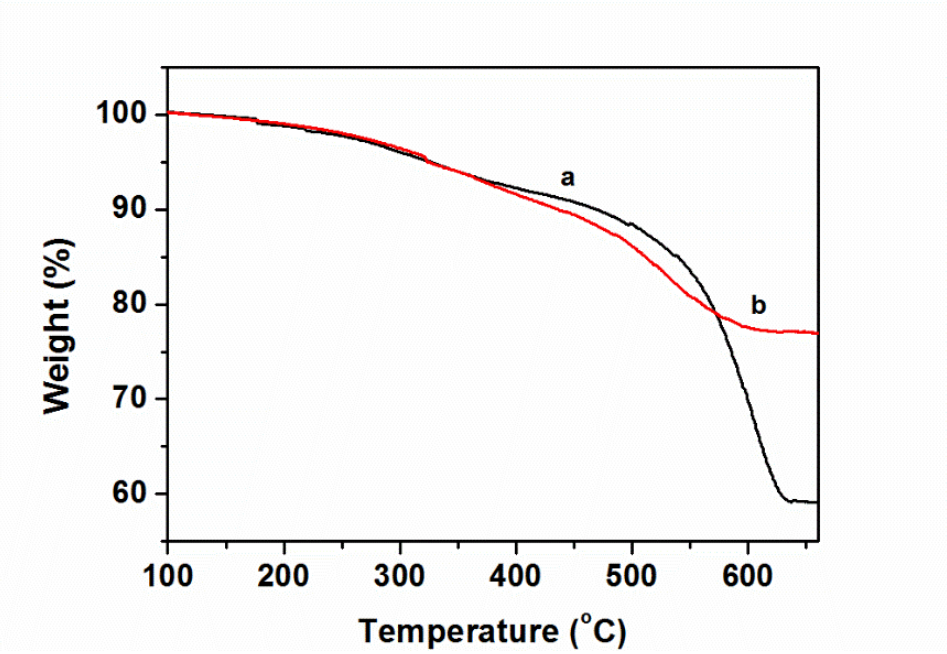

Figure 1.8 TG curves of spent Ni/Q-30 (a) and Ni/ZrO_2-SiO_2-B (b) bimodal catalyst after 6 h of reaction.

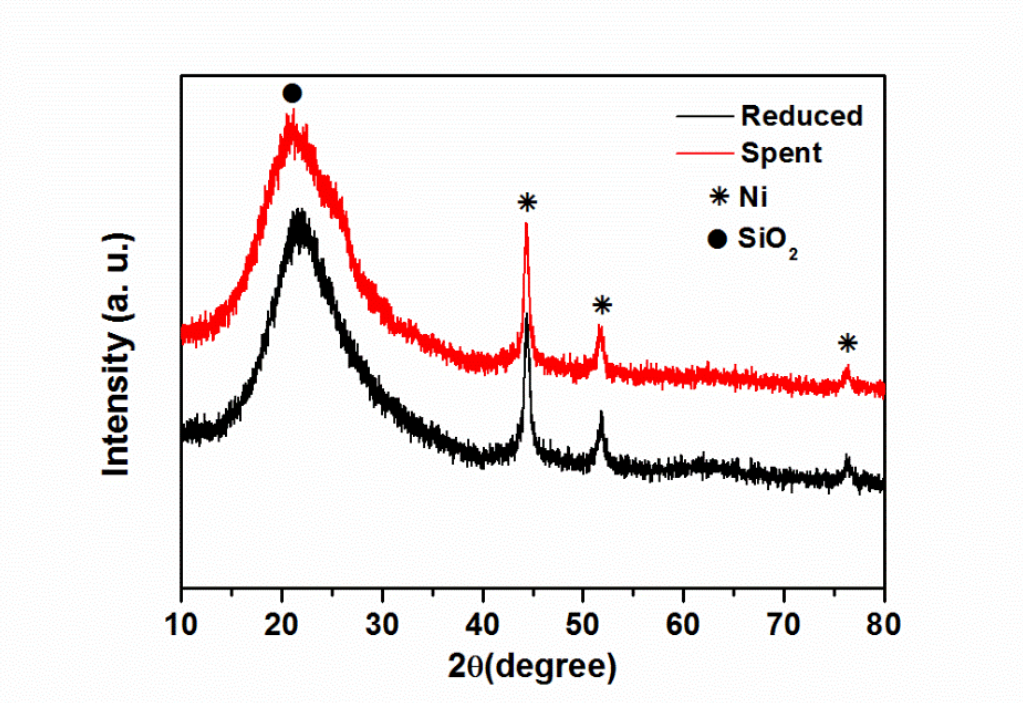

Figure 1.9 XRD patterns of reduced and spent Ni/ZrO_2-SiO_2-B bimodal catalyst.

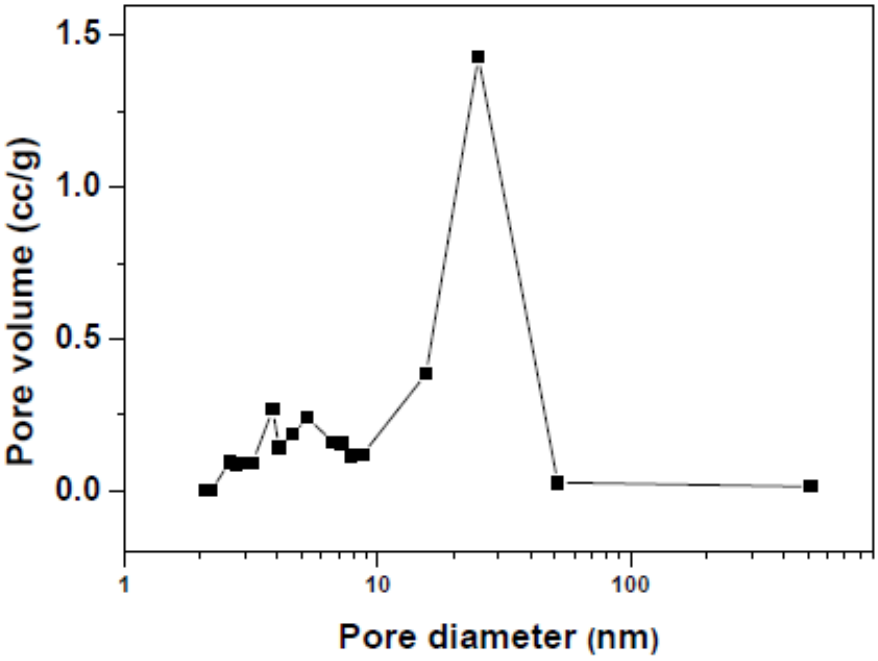

Figure 1.10 Pore size distribution of spent Ni/ZrO_2-SiO_2-B bimodal catalyst.

Chapter 2

Direct Synthesis of Liquefied Petroleum Gas from Syngas over H-ZSM-5 Enwrapped Pd-based Zeolite Capsule Catalyst

The millimeter-sized zeolite capsule catalyst (Pd/SiO_2-SZ) with a core-shell structure was prepared by a developed dual-layer crystal growth method. The prepared Pd/SiO_2-SZ zeolite capsule catalyst illustrated excellent LPG selectivity for the direct synthesis of liquefied petroleum gas from syngas.

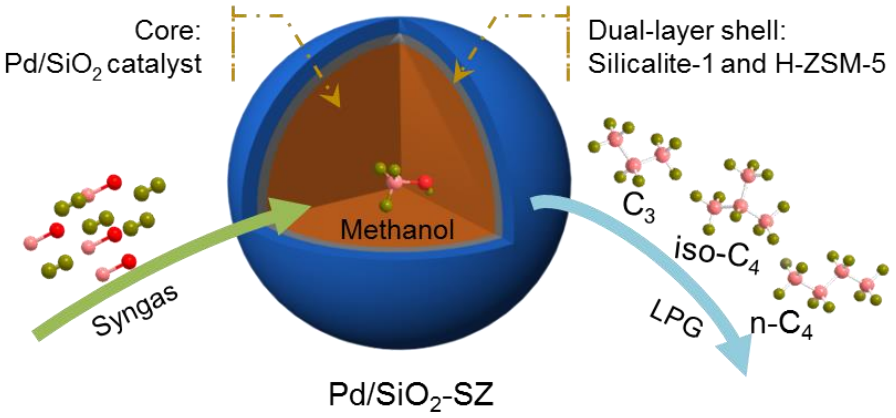

Abstract

A facile synthesis route, named dual-layer crystal growth method, was developed for preparing Pd-based zeolite capsule catalyst. The millimeter-sized zeolite capsule catalyst (Pd/SiO_2-SZ) with a core-shell structure was prepared by a developed dual-layer crystal growth method: coating Silicalite-1 and H-ZSM-5 zeolite orderly as double shells encapsulating the Pd/SiO_2 core catalyst. We employed the prepared Pd/SiO_2-SZ zeolite capsule catalyst for the direct synthesis of liquefied petroleum gas (LPG) from syngas ($CO+H_2$). In the reaction, the zeolite capsule catalyst showed excellent LPG selectivity than the single core catalyst of Pd/SiO_2 and the physical mixture catalyst prepared by a simply mixing core and shell catalysts. The Pd/SiO_2-SZ realized the highest LPG selectivity of 34.4% with CO conversion of 14.1%. Moreover, the optimal reaction temperature and pressure in the reaction for LPG direct synthesis from syngas over Pd/SiO_2-SZ catalyst were 623 K and 5.0 MPa, respectively. The high performance of zeolite capsule catalyst Pd/SiO_2-SZ was attributed to the enforced mass transfer diffusion from inside to outside of the catalyst.

Keywords: Zeolite capsule catalyst, Liquefied petroleum gas, Pd-based catalyst, Syngas, Zeolite membrane

2.1. Introduction

Currently, the global energy crisis and environmental contamination issues are greatly concerned in the world. More works about exploring green energy have been studied for several decades. For instance, liquefied petroleum gas (LPG), a mixture of propane and butane, is widely regarded as a promising candidate for fuel in household and industry fields duo to its excellent chemical characteristic such as clean, renewable and easy storage [1-6]. LPG is mainly obtained from petroleum refining, natural gas and crude oil exploration [7]. The direct synthesis of valued-hydrocarbons from non-petroleum resource is a promising technology due to the declining of petroleum reserves.

Syngas as a type of non-petroleum resource, a mixture of CO and H_2, is produced from natural gas, biomass and coal. It is an essential platform to transform the lower carbon resource into high-value-added products [8-12]. Among the process of syngas conversion to hydrocarbons, there are two primarily catalytic approaches: Fischer-Tropsch synthesis (FTS) and syngas-methanol-hydrocarbons synthesis in current situation [13]. FTS is a traditional process to produce hydrocarbons through syngas transformation. However, the products are limited by Anderson-Schulz-Flory (ASF) law distribution. FTS is non-selective to any specific hydrocarbon species and contains low selectivity of light hydrocarbons if without further catalysts modification [14,15]. As a catalytic approach different from FTS, the light alkanes and olefins can be precisely synthesized from syngas via methanol as intermediate over bifunctional catalyst, containing methanol synthesis catalyst and acidic zeolite [16-19]. In addition, the products distribution in this route does not obey ASF distribution. A successful issue was pioneered by Mobil for achieving high octane gasoline. In this process, methanol is firstly synthesized from syngas, followed by its conversion to gasoline over H-ZSM-5 zeolite in the methanol-to-gasoline (MTG) process [20].

Palladium (Pd) has been used as an active catalyst for syngas conversion to methanol since 1978 due to its high selectivity of methanol [21]. Furthermore, Pd-based catalyst has high methanol selectivity under higher reaction temperature, compared with $Cu/ZnO/Al_2O_3$ and ZnO/Cr_2O_3 catalysts [22,23]. As known, the formation of dimethy ether (DME) and higher hydrocarbons from methanol requires acidic sites in the catalyst. Hence, several zeolites, such as H-ZSM-5, H-β and H-Y materials, are used as acidic catalysts for methanol dehydration into hydrocarbons [24-26]. Recently, some reports have developed mixture catalyst, which contains methanol synthesis catalyst and zeolite catalyst, to overcome the thermodynamic equilibrium limitation of syngas to methanol [18]. However, zeolite capsule catalyst with core-shell structure has attracted great concern in many research fields especially in catalysis, because the different active sites of catalyst are organized in a unified and ordered architecture, which makes its better catalytic performance in various catalysis reactions [27-30].

It is reported that the acidic properties and channel architecture of zeolite determine the catalytic activity and products selectivity [31,32]. H-ZSM-5 zeolite has been frequently used as dehydration catalyst to realize hydrocarbons synthesis through methanol dehydration [33]. Recently, a series of H-ZSM-5 based zeolite capsule catalysts have been systematically studied and demonstrated higher selectivity than the conventional mixture catalysts for iso-paraffin synthesis in FTS reactions [34,35]. These zeolite capsule catalysts with a special core-shell structure exhibited confined reaction environment, by which to realize excellent catalytic performance in the reactions. Moreover, excellent DME selectivity was achieved over the well-designed zeolite capsule catalysts in the reaction of syngas to dimethyl ether (STD) [36,37]. These extraordinary achievements revealed that the well-fined and ordered structure of catalysts can enhance the catalytic performance effectively. Therefore, the application of syngas direct conversion to LPG over core-shell structured catalyst is desirable.

In this paper, we developed a facile method for coating Silicalite-1 and H-ZSM-5 zeolite orderly as double shells on the Pd/SiO_2 pellet (Pd/SiO_2-SZ). The physical properties of zeolite capsule catalyst were determined by XRD and SEM characterization. The as-prepared Pd/SiO_2-SZ zeolite capsule catalyst was evaluated in the reaction of syngas direct conversion to LPG. The different reaction conditions of Pd/SiO_2-SZ zeolite capsule catalyst on catalytic performance were also investigated.

2.2. Experimental section

2.2.1 Catalyst preparation

2.1.1.1 Preparation of Pd/SiO_2 core catalyst

The core catalyst of Pd/SiO_2 was prepared by incipient wetness impregnation method. Silica pellets (Cariact Q10 0.85-1.7 mm) were loaded with 5 wt% of Pd, using $Pd(NH_3)_2(NO_3)_2$ aqueous solution under ultrasonic agitation for 30 min. The obtained sample was dried at 393 K overnight and followed by calcination at 673 K for 3 h in air.

2.1.1.2 Synthesis of Pd/SiO_2-S capsule catalyst

We prepared the capsule catalyst by coating Silicalite-1 and H-ZSM-5 zeolite shells on the Pd/SiO_2 pellets successively. The Silicalite-1 zeolite shell was first synthesized on the surface of Pd/SiO_2 pellets by hydrothermal synthesis as a protective layer. Briefly, the recipe for Silicalite-1 zeolite synthesis was 2TEOS: 0.48TPAOH: $120H_2O$: 8EtOH: $0.024HNO_3$. The precursor compounds were mixed until clear solution was achieved. Then the mother liquid was moved into a teflon reactor and sealed in an autoclave with Pd/SiO_2 pellets together. The hydrothermal treatment was performed in hydrothermal synthesis reactor at 453 K for 24 h. After crystallization, the product was filtrated by centrifugation, and washed by deionized water several times until the pH of product reached 7. Finally, the sample was obtained by drying after 393 K in oven for 12 h and calcination at 773 K in muffle for 5 h with heating rate of 1 K/min. The obtained capsule catalyst was named as Pd/SiO_2-S, where the S means

Silicalite-1 shell.

2.1.1.3 Synthesis of Pd/SiO_2-SZ capsule catalyst

The Pd/SiO_2-S catalyst was used as core catalyst for the successive H-ZSM-5 zeolite shell growth. The recipe of H-ZSM-5 zeolite synthesis solution was 2TEOS: 0.68TPAOH: $120H_2O$: 8EtOH: $0.024Al_2O_3$, where $Al(NO_3)_3{\cdot}9H_2O$ served as aluminum source. Firstly, the resulted solution was mixed by stirring for 4 h at room temperature to form homogeneous gel. The prepared Pd/SiO_2-S catalyst was immersed in this H-ZSM-5 synthesis solution and sealed in hydrothermal synthesis reactor at 453 K for 24 h. After crystallization, the product was filtrated by centrifugation and washed by deionized water several times. Finally, the sample was obtained by drying at 393 K in oven for 12 h and calcination at 773 K in muffle for 5 h with heating rate of 1 K/min. The obtained capsule catalyst was denoted as Pd/SiO_2-SZ, where the S means Silicalite-1 shell and Z stands for H-ZSM-5 shell. The weight of zeolite shell encapsulating on the Pd/SiO_2-SZ catalyst was calculated to be 16.7 wt%.

2.1.1.4 Preparation of Pd/SiO_2-M catalyst

The reference catalyst of Pd/SiO_2-M was derived from Pd/SiO_2-SZ zeolite capsule catalyst through regrinding way, which made the constituents and weight ratio of this reference catalyst were consistent with those of the Pd/SiO_2-SZ zeolite capsule catalyst. The above-prepared Pd/SiO_2-SZ capsule catalyst was grinded into powder, and then re-prilled into new particles with a size of 0.85-1.70 mm. The M stands for the physical mixture.

2.2.2 Catalyst characterization

X-ray diffraction (XRD) patterns of the catalysts were analyzed by a Rigaku RINT 2400 X-ray Diffractometer equipped with a Cu Kα radiation (λ=1.5406Å). Scans were recorded in the 2θ range of 5-90^o with a step size of 0.02 ^{o}/s. All samples were grinded to powder before characterization.

The Brunauer-Emmett-Teller (BET) surface area, micropore volume and average pore size of the prepared catalysts were determined by N_2 physical adsorption at 77 K and measured using Micromeritics 3Flex specific surface area and porous physical adsorption analyzer. All samples were degassed in vacuum at 473 K for 3 h before measurement.

SEM images and surface elemental composition of samples were obtained by a JEOL JSM-6360LV scanning electron microscope equipped with JED-2300 energy dispersive spectroscopy (EDS) attachment.

The X-ray photoelectron spectroscopy (XPS) analysis was done by Thermo Fisher Scientific ESCALAB 250Xi multifunctional X-ray photoelectron spectroscope and the data processing was performed using Avantage software.

NH_3 temperature programmed desorption (NH_3-TPD) was conducted by a catalyst analyzer BELCAT-B-TT (BEL Japan Co. Ltd.) equipped with a thermal conductivity detector (TCD). 0.03 g catalyst was pretreated at 423 K in He flow for 1 h, then 5% NH_3 in He was introduced for 1 h with flow rate of 20 ml/min while temperature was cooling down to 353 K. Subsequently, the microreactor was purified with pure He for 1 h. Finally, the NH_3 desorption procedure was proceeded in He flow (30 ml/min) by increasing the temperature from room temperature to 1073 K with a ramping rate of 5 K/min.

Thermogravimetry (TG) analysis was performed on DTG-60 DTA-TG apparatus (Shimadzu Corporation, Japan). 10 mg spent catalyst was heated in air with flow rate of 30 ml/min. The progress was performed at the condition of 10 K/min heating rate from room temperature to 1173 K.

2.2.3 Catalytic performance test

The catalytic performance in the synthesis of LPG from syngas over various catalysts was carried out in a fixed-bed steel reactor with inner diameter of 6 mm. Prior to the test, all catalysts were reduced in the reactor for 10 h at 673 K with high-purity H_2.

After cooling to room temperature, syngas containing CO_2, with a H_2/CO molar ratio of 2, was introduced into the reactor. Then, the reaction was conducted under the required conditions. The effect of reaction temperature (573, 623 and 673 K) and pressure (2.0, 3.0 and 5.0 MPa) on catalytic performance were investigated. All products in the gas phase from the reactor outlet were analyzed by an on-line GC-8A gas chromatograph (GC, Shimadzu Corporation, Japan), which was equipped with Plot S column for the thermal conductivity detector (TCD), and HP-PLOT/Q column for the flame ionization detector (FID). The CO conversion and the products selectivity were calculated as the followed equations.

$$\begin{aligned} &C_{CO} = (X_{CO,in} - X_{CO,out})/(X_{CO,in}) \times 100\% \\ &C_{CO} : \text{Conversion of CO, \%;} \\ &X_{CO,in} : \text{Mole fraction of CO in pristine syngas;} \\ &X_{CO,out} : \text{Mole fraction of CO in exit gas;} \end{aligned} \tag{2-1}$$

$$\begin{aligned} &C_{CO2} = (X_{CO2,in} - X_{CO2,out})/(X_{CO2,in}) \times 100\% \\ &C_{CO2} : \text{Conversion of } CO_2\text{, \%;} \\ &X_{CO2,in} : \text{Mole fraction of } CO_2 \text{ in pristine syngas;} \\ &X_{CO2,out} : \text{Mole fraction of } CO_2 \text{ in exit gas;} \end{aligned} \tag{2-2}$$

$$\begin{aligned} &Sel_i = \frac{R_{i,s} f_{i,m}}{\sum_i R_{i,s} f_{i,m}} \\ &Sel_i : \text{Mass selectivity of component i, \%;} \\ &f_{i,m} : \text{Factor of mass correction;} \\ &R_{i,s} : \text{Area ratio of product in GC} - \text{FID.} \end{aligned} \tag{2-3}$$

2.3. Results and discussion

2.3.1 Structure and characterization of the catalysts

The BET specific surface areas, pore volumes, and average pore diameters of these catalysts are summarized in Table 2.1. The specific surface area decreases from 294.4 m^2/g of SiO_2 to 230.5 m^2/g of Pd/SiO_2 since the palladium metal deposition in the SiO_2 pores. The specific surface area and micropore surface area of zeolite capsule catalysts

increase slightly due to the growth of zeolite shell. It confirms that the microporous zeolite was formed in the capsule catalysts. The capsule catalysts Pd/SiO_2-SZ, Pd/SiO_2-S and mixture catalyst Pd/SiO_2-M have lower pore volume in relative to Pd/SiO_2 core catalyst, because few zeolite synthesis solution entered the pore of Pd/SiO_2 core catalyst during hydrothermal synthesis.

The XRD diffraction patterns of the H-ZSM-5 zeolite, Pd/SiO_2 core catalyst, Pd/SiO_2-M mixture catalyst, Pd/SiO_2-S and Pd/SiO_2-SZ zeolite capsule catalysts are presented in Figure 2.1. It is clear that the broad diffraction peaks of amorphous SiO_2 and diffraction peaks of PdO are presented in the Pd/SiO_2 catalyst. Moreover, the energy dispersive spectroscopy (EDS) analysis result illustrates that loaded Pd is close to 5 wt% (Figure 2.2b). For the Pd/SiO_2-S and Pd/SiO_2-SZ zeolite capsule catalysts, the diffraction peaks of PdO and amorphous SiO_2 are also identified, indicating that the SiO_2 support is retained completely because of the protection of Silicalite-1 shell. Moreover, the PdO particle size is similar for all of the catalysts as listed in the Table 2.1. It suggests that the hydrothermal synthesis treatment for zeolite shell synthesis does not affect the PdO particle size in the Pd/SiO_2. The XRD patterns of Pd/SiO_2-S and Pd/SiO_2-SZ zeolite capsule catalysts show typical peaks of MFI type zeolite in the ranges of 2θ=7~9° and 22~25°. The results imply that Silicalite-1 and H-ZSM-5 zeolite shells are successfully formed on the Pd/SiO_2.

The surface morphology and elemental analysis of different catalysts are determined by SEM micrograph and EDS analysis. Pd/SiO_2 core catalyst presents a comparatively smooth surface as shown in the Figure 2.2a. The Si Kα, O Kα and Pd Kα can be found on the surface of Pd/SiO_2 core catalyst, and the loading Pd amount of catalyst is close to the designed amount. Herein, the spherical structure of Pd/SiO_2 catalyst is used as the core of catalyst for zeolite capsule catalyst preparation by coating the Silicalite-1 and H-ZSM-5 zeolite shells orderly during the hydrothermal synthesis.

The surface SEM images and EDS analysis results of Pd/SiO_2-S capsule catalyst are shown in Figure 2.3. The formed Silicalite-1 zeolite shell presents a relative roughness on the exterior surface of Pd/SiO_2-S catalyst and Pd elements are hardly observed, suggesting that Silicalite-1 zeolite shell enwrapped the Pd/SiO_2 core catalyst. The morphology of Silicalite-1 zeolite is irregular with long hexagon shape. The function of Silicalite-1 zeolite shell between core Pd/SiO_2 and H-ZSM-5 zeolite shell is not only to protect SiO_2 support from etching in strong alkaline of H-ZSM-5 synthesis liquid, it is also used as crystal seed for growth of H-ZSM-5 zeolite shell [37,38]. The cross-section SEM image and relative element concentration of Si and Pd by EDS line scans for Pd/SiO_2-S capsule catalyst are shown in Figure 2.3c and 2.3d, respectively. Approximately 11 μm thickness of Silicalite-1 zeolite shell can be found in cross-section SEM image (Figure 2.3c), which further suggests that the perfect Silicalite-1 shell is successfully prepared. In addition, no corrosion on the Pd/SiO_2 core catalyst is observed through Silicalite-1 shell synthesis. Thus, the Pd/SiO_2 are stable under hydrothermal condition for Silicalite-1 shell. The corresponding EDS line analysis is simultaneously obtained along the red line in the SEM image from core to zeolite shell. The Si signal decreases in the boundary of core catalyst and zeolite shell and then increases in the zeolite shell, indicating the change from the core catalyst to shell.

The Pd/SiO_2-SZ zeolite capsule catalyst is established by H-ZSM-5 zeolite shell coating on the Pd/SiO_2-S. The morphology features and elements analysis of the Pd/SiO_2-SZ zeolite capsule catalyst are given by the surface SEM image and EDS analysis in the Figure 2.4a and 2.4b. The H-ZSM-5 zeolite crystal having hexagonal shape with the round corner is observed in Figure 2.4a, which is slightly different to that of Silicalite-1. The results of external surface EDS analysis of Pd/SiO_2-SZ zeolite capsule catalyst are shown in the Figure 2.4b. After the encapsulation of zeolite shell, Pd cannot be detected, indicating that the double shells are compact and uniform.

Additionally, the Si/Al molar ratio of H-ZSM-5 zeolite shell (Si/Al = 33.9) can be obtained by EDS analysis. Figure 2.4c and 2.4d show the SEM cross-section image and elemental distribution of the encapsulated Pd/SiO_2 pellet. There is a clear distinction between Pd/SiO_2 pellet and zeolite shell as demonstrated in the cross-section SEM image. Meanwhile, there is no change for Pd/SiO_2 core catalyst after H-ZSM-5 coating in further hydrothermal synthesis process. It can be observed that a typical and tight zeolite shell is synthesized on the surface of Pd/SiO_2 pellet. The thickness of dual zeolite shells is up to 26 μm. However, the boundary between Silicalite-1 and H-ZSM-5 cannot be clearly observed by SEM image. Because both the Silicalite-1 and H-ZSM-5 zeolite belong to the MFI-type zeolite with the same three-dimensional pore structure and analogous chemical composition. H-ZSM-5 zeolite is epitaxially synthesized on the surface of the Silicalite-1 layer, which leads to a direct pore to pore connection between H-ZSM-5 and Silicalite-1 [37,39,40]. Therefore, the radial distribution of Al Kα is used to detect the boundary between Silicalite-1 and H-ZSM-5 from the EDS analysis. The change of Al Kα, Si Kα and Pd Kα from the core to zeolite shell is listed in Figure 2.4d. At the interface region between core catalyst and zeolite shell, the radial distribution of Al Kα increases slightly, indicating that the double zeolite layers encapsulate the core catalyst. From the analysis results of SEM image and EDS radial distribution profiles, we can find that the H-ZSM-5 zeolite shell thickness of Pd/SiO_2-SZ is about 15 μm.

In order to further demonstrate the change of Pd nanoparticles on the core catalyst before and after the hydrothermal synthesis, the XPS surface technology is applied. XPS is a sensitive surface chemical analysis technique to determine the chemical composition of different catalysts in the near-surface regions. XPS spectra of different catalysts with survey spectrum and high-resolution of Pd are illustrated in the Figure 2.5. The primary spectra of Pd 3d, Si 2p, O 1s and C 1s are obtained from the XPS survey (Figure 2.5a). The Pd $3d_{5/2}$ binding energy of 336~336.5 eV is ascribed to PdO species [28,41]. For the Pd/SiO_2 core catalyst and Pd/SiO_2-S capsule catalyst, the Pd 3d spectra

exhibits double peaks with binding energy at 336.1 eV and 342.4 eV, corresponding to Pd $3d_{5/2}$ and Pd $3d_{3/2}$, respectively. For the Pd/SiO_2-SZ capsule catalyst, no Pd 3d spectra peaks are detected, suggesting that no Pd element exists on the surface of capsule catalyst. The XPS analysis results reveal the surface compositions of the catalysts, as shown in Table 2.1. The atomic weight of Pd on the Pd/SiO_2-SZ zeolite layer is zero, indicating that the dual zeolite layers are integrity and fully encapsulate the core Pd/SiO_2.

The acidic properties of the zeolite shell will clearly affect the catalytic performances of capsule catalyst. The NH_3-TPD profiles of the zeolite and various catalysts are shown in Figure 2.6. Obviously, no NH_3 desorption peak is observed on the naked Pd/SiO_2 core catalyst and Pd/SiO_2-S, which means that there are no acidic sites on these catalysts. For the pure H-ZSM-5 zeolite, two desorption peaks at 473 K and 750 K are clearly observed, which are corresponded to the weak and strong acid sites, respectively [8,42]. For the Pd/SiO_2-SZ capsule catalyst, one peak for NH_3 desorption appears at 450 K, because of the NH_3 desorption from the weak acidic sites. The weak acidic sites as active phase are very crucial for methanol dehydration to form hydrocarbons. Thus, for the zeolite capsule catalyst, the H-ZSM-5 zeolite shell with appropriate active sites is beneficial to its catalytic performance for LPG direct synthesis from syngas.

2.3.2 Catalytic reaction performance comparison

The synthesis of LPG from syngas containing CO_2 with methanol as intermediate is a tandem catalysis process. This tandem reaction possesses a series of catalysis reaction procedures: CO hydrogenation to form methanol and methanol further dehydration to hydrocarbons including LPG over the zeolite catalysts. Here, Pd/SiO_2-SZ zeolite capsule catalyst is used to investigate the catalytic performance for direct synthesis of LPG from syngas. Syngas, passing through shell, is first converted to methanol by the Pd/SiO_2 core of capsule catalyst, then the hydrocarbons are formed by

methanol dehydration during the diffusion inside zeolite shell. The Pd/SiO_2-S and Pd/SiO_2-M, as reference catalysts, are also tested in this reaction. In addition, the effect of reaction temperature and pressure on catalyst performance is also investigated.

The catalytic performances of Pd/SiO_2, Pd/SiO_2-S, Pd/SiO_2-SZ and Pd/SiO_2-M catalysts in LPG synthesis reaction, are listed in Table 2.2. The Pd/SiO_2-SZ zeolite capsule catalyst shows CO conversion of 14.1%, which is higher than Pd/SiO_2-S capsule catalyst but it is lower than Pd/SiO_2 core catalyst and Pd/SiO_2-M mixture catalyst. The zeolite shell covers partial active sites on the surface of Pd/SiO_2 core catalyst, which may lead to the lower CO hydrogenation activity of zeolite capsule catalyst than that of Pd/SiO_2 core catalyst. The exposed active sites on Pd/SiO_2-M catalyst result in higher CO conversion in LPG synthesis. The Pd/SiO_2-M mixture catalyst is derived from restructuring the Pd/SiO_2-SZ zeolite capsule catalyst by breaking the core-shell architecture.

The CO_2 in the syngas feed gas participates in methanol synthesis by its hydrogenation and it can be also produced from CO through Water-Gas-shift (WGS) reaction over metal active site. Many researches have demonstrated that introducing CO_2 into syngas can influence the CO hydrogenation reaction [38,43]. In this LPG synthesis reaction, the CO_2 conversion is decreased from Pd/SiO_2, Pd/SiO_2-S to Pd/SiO_2-SZ in order. The zeolite shell covers partial active sites on the surface of Pd/SiO_2 core catalyst, which may lead to the lower CO and CO_2 hydrogenation activity of zeolite capsule catalyst than that of Pd/SiO_2 core catalyst. Moreover, the Silicatlite-1 shell is inert and hydrophobic zeolite material, which efficiently depresses the WGS reaction. The diffusion resistance of syngas passing through zeolite shell should also be considered. The exposed active sites on Pd/SiO_2-M catalyst result in higher CO conversion while lower CO_2 conversion in LPG synthesis. The lower conversion of CO_2 over the Pd/SiO_2-M is ascribed to the formation of more CO_2 by WGS reaction. More exposed Pd sites on the Pd/SiO_2-M catalyst will make WGS reaction more active.

The products distribution exhibits a significant difference among these catalysts, as compared in Table 2.2. Methanol (MeOH) is the major product of Pd/SiO_2 core catalyst. Besides, the few hydrocarbons are formed over the Pd/SiO_2 core catalyst. The SiO_2 support is not absolutely neutral, and it possesses very low acidic sites which are enough to dehydrate few methanol into alkanes/alkenes under available reaction conditions. The result is also consistent with the literature [44]. For the Pd/SiO_2-S capsule catalyst, the methane is the main product and its selectivity reaches up to 59.8%. Silicalite-1 is a non-acidic zeolite, which leads to the lower yield of C_{2+} hydrocarbons. Moreover, the high temperature promotes the CO alkylation on the Pd active site, which results in high selectivity of methane [16]. The higher methanol selectivity on the Pd/SiO_2-S is ascribed to the incomplete dehydrogenation of methanol over the non-acidic Silicalite-1, therefore leading to the accumulation of methanol in the final products. In addition, the ethane selectivity is increased from Pd/SiO_2, Pd/SiO_2-S, Pd/SiO_2-M to Pd/SiO_2-SZ in order. The results indicate that introducing zeolite with strong acidic sites can clearly change the products distribution towards the formation of light alkanes, like ethane and propane. Even though the Pd/SiO_2-M catalyst has slightly higher CO conversion, the LPG selectivity of Pd/SiO_2-SZ catalyst is much higher than that of Pd/SiO_2-M catalyst. Pd/SiO_2-SZ zeolite capsule catalyst realizes as high as 34.4% LPG selectivity with little amount of MeOH and DME. The reaction environment suitable for LPG synthesis can be fabricated in the confined structure of Pd/SiO_2-SZ zeolite capsule catalyst with the advantage of the promoted mass and heat transfer.

It is considered that without the confined reaction regulation, as for random distribution of methanol synthesis catalyst and zeolite catalyst in Pd/SiO_2-M physical mixture catalyst, a part of MeOH and DME, as intermediate, have no enough chance to be converted to hydrocarbons on the neighboring zeolite. Consequently, MeOH and DME selectivities are high as shown in Table 2.2. On the other hand, with the

tailor-made confinement reaction field design in the Pd/SiO_2-SZ zeolite capsule catalyst, all the MeOH and DME produced by the core catalyst, are guaranteed enough chances to be transformed to hydrocarbons on the acidic sites when they pass the zeolite membrane channels, determining very high hydrocarbons selectivity by suppressing MeOH and DME selectivity.

The carbon deposition on the catalysts during the reaction mainly affects the catalyst life time. TG is employed to determine the coke deposition amount on the spent catalysts, and the weight loss rate of different spent catalysts is shown in the Figure 2.7. The weight loss below 473 K is attributed to the adsorbed water, and the weight loss above 750 K is attributed to coke-related species [45,46]. For the naked Pd/SiO_2 core catalyst, the weight loss is found only in the lower temperature region, which is attributed to the adsorbed water or gases. In the higher temperature region, there is almost no weight loss on the Pd/SiO_2 core catalyst, indicating the near-zero carbon species deposition. Moreover, the weight loss amount caused by carbon deposition on the zeolite capsule catalyst Pd/SiO_2-SZ is lower than that of mixture catalyst Pd/SiO_2-M, suggesting that the formation of carbonaceous species on the Pd/SiO_2-SZ catalyst is suppressed obviously.

2.3.3 Catalytic performance of Pd/SiO_2-SZ zeolite capsule catalysts for LPG synthesis

Reaction temperature is essential for the CO hydrogenation and products distribution. Table 2.3 shows the effect of temperature on LPG synthesis over Pd/SiO_2-SZ zeolite capsule catalyst. The CO conversion illustrates an increment with the increase of reaction temperature. The CO conversion of Pd/SiO_2-SZ zeolite capsule catalyst is 9.0% at 573 K and it arises to 15.2% when the temperature reaches to 673 K. The temperature is also crucial to the products distribution of hydrocarbons. Although lower reaction temperature is beneficial to the formation of methanol from syngas, it is not helpful to the dehydration of the formed methanol generating LPG. Excessively high temperature is not appropriate for methanol synthesis due to the limitation of

thermodynamic equilibrium. But it can accelerate CO methanation reaction over Pd/SiO_2 catalyst, therefore leading to the formation of methane as predominant product at 673 K [16]. In addition, the slightly higher methanol selectivity on the Pd/SiO_2-SZ at 673 K is ascribed to the incomplete dehydrogenation of methanol over the zeolite shell, therefore leading to the accumulation of methanol in the final products. The maximum selectivity of LPG over Pd/SiO_2-SZ zeolite capsule catalyst is 34.4% at 623 K Therefore, the optimal temperature for LPG synthesis using Pd/SiO_2-SZ zeolite capsule catalyst is 623 K, at which the highest selectivity of LPG and lower selectivity of byproducts are achieved.

The effect of reaction pressure on the catalytic performance over Pd/SiO_2-SZ zeolite capsule catalyst is presented in Table 2.4. Increasing reaction pressure can enhance CO conversion and promote methanol formation [25]. Therefore, the formed methanol will be further converted into hydrocarbons including LPG under the appropriate temperature (623 K), which leads to the decreased methanol selectivity. The selectivity of LPG reaches up to 34.4% under the reaction pressure of 5.0 MPa. Moreover, the formation of methane can be effectively depressed under high reaction pressure due to the accelerated C-C bond formation rate. The selectivity of methane is 35.3% under the reaction pressure of 2.0 MPa; it is reduced to 24.3% by increasing the reaction pressure to 5.0 MPa. Hence, the reaction pressure of 5.0 MPa, also the optimized reaction pressure for methanol synthesis, is suitable for the LPG direct synthesis from syngas over Pd/SiO_2-SZ zeolite capsule catalyst.

The catalyst life time is one of important catalytic performances of zeolite capsule catalyst. The time on stream of CO conversion and LPG selectivity over Pd/SiO_2-SZ are presented in Figure 2.8. The Pd/SiO_2-SZ capsule catalyst demonstrates excellent stability with enhanced CO conversion of 14% and LPG selectivity of 34% during 100 h reaction time. The outstanding catalytic stability of Pd/SiO_2-SZ capsule catalyst is attributed to its core-shell structure.

2.4. Conclusions

In summary, a Pd/SiO_2-SZ zeolite capsule catalyst is prepared by a developed dual-layer growth method. The catalyst characterization demonstrates that the Pd/SiO_2-SZ zeolite capsule catalyst has millimeter-sized core-shell structure with a compact H-ZSM-5 shell. Pd/SiO_2-SZ zeolite capsule catalyst is used to investigate the catalytic performance of direct LPG synthesis from syngas. In addition, the effect of reaction temperature and pressure on the catalytic performance of the Pd/SiO_2-SZ zeolite capsule catalyst for syngas converting to LPG has also been investigated. In contrast to the naked Pd/SiO_2 core catalyst and the mixture catalyst Pd/SiO_2-M, the zeolite capsule catalyst shows excellent LPG selectivity. The LPG selectivity on this Pd/SiO_2-SZ zeolite capsule catalyst reaches 34.4% with CO conversion of 14.1%. The unexpected superior performance of Pd/SiO_2-SZ zeolite capsule catalyst is ascribed to the tailor-made core-shell-like structure, which provides a confined reaction environment for LPG direct synthesis from syngas. The new findings in this study are beneficial to designing core-shell-like catalysts for LPG direct synthesis from syngas, and the presented catalyst preparation method in this paper can be also extended to other tandem catalysis processes.

References

[1] H.E. Saleh, Fuel, 2008, 87, 3031-3039.

[2] X. Zou, X. Wang, L. Li, K. Shen, X. Lu, W. Ding, Int. J. Hydrogen Energy, 2010, 35, 12191-12200.

[3] S. Kim, M.K. Mayeda, E. Sasmaz, J. Lauterbach, ACS Sustain. Chem. Eng., 2015, 3, 381-385.

[4] X. Ma, Q. Ge, J. Ma, H. Xu, Fuel Process. Technol., 2013, 109, 1-6.

[5] D. Qi, Y. Bian, Z. Ma, C. Zhang, S. Liu, Energy Convers. Manage., 2007, 48, 500-509.

[6] G. Lu, L. Li, Energy Procedia, 2011, 12, 897-905.

[7] Q. Zhang, X. Li, K. Asami, S. Asaoka, K. Fujimoto, Fuel Process. Technol., 2004, 85, 1139-1150.

[8] J. Sun, X. Li, A. Taguchi, T. Abe, W. Niu, P. Lu, Y. Yoneyama, N. Tsubaki, ACS Catal., 2014, 4, 1-8.

[9] M. A. Pena, J. P. Gómez, J. L. G. Fierro, Appl. Catal. A: Gen., 1996, 144, 7-57.

[10] M. Asadullah, S.I. Ito, K. Kunimori, M. Yamada, K. Tomishige, J. Catal., 2002. 208, 255-259.

[11] V. Subramani, S.K. Gangwal, Energy and Fuels, 2008, 22, 814-839.

[12] P. Taylor, Catal. Rev. Sci. Eng., 1987, 29, 361-445.

[13] G.P.V. Der Laan, A.A.C.M. Beenackers, Catal. Rev. Sci. Eng., 1991, 41, 255-318.

[14] H.M.T. Galvis, J.H. Bitter, C.B. Khare, M. Ruitenbeek, A. lulian Dugulan, K.P. de Jong, Science, 2012, 335, 835-838.

[15] C. Xing, G. Yang, P. Lu, W. Shen, X. Gai, L. Tan, J. Mao, T. Wang, R. Yang, N. Tsubaki, Microporous Mesoporous Mater., 2016, 233, 62-69.

[16] Q. Zhang, X. Li, K. Asami, S. Asaoka, K. Fujimoto, Catal. Today, 2015, 104, 30-36.

[17] Q. Zhang, T. Ma, M. Zhao, T. Tomonobu, X. Li, Catal. Sci. Technol., 2016, 6, 1523-1529.

[18] F.A.P. Cavalcanti, A.Y. Stakheev, W.M.H. Sachtler, J. Catal., 1992, 134, 226-241.

[19] J. Sun, G. Yang, Y. Yoneyama, N. Tsubaki, ACS Catal., 2014, 4, 3346-3356.

[20] C.D. Chang, Catal. Rev. Sci. Eng., 1983, 25, 1-118.

[21] M. L. Poutsma, L.F. Elek, P.A. Ibarbia, J.A. Rabo, J. Catal., 1978, 52, 157-168.

[22] J. M. Driessen, E.K. Poels, J.P. Hindermann, V. Ponec, J. Catal., 1983, 82, 26-34.

[23] N. Tsubaki, K. Fujimoto, Top. Catal., 2003, 22, 325-335.

[24] K. Fujimoto, H. Saima, H. Tominaga, Bull. Chem. Soc. Jpn., 1988, 2547-2550.

[25] Q. Ge, X. Li, H. Kaneko, K. Fujimoto, J. Mol. Catal. A Chem., 2007, 278, 215-219.

[26] X. Ni, Y. Tan, Y. Han, N. Tsubaki, Catal. Commun., 2007, 8, 1711-1714.

[27] H. Wang, L. Chen, Y. Feng, H. Chen, Acc. Chem. Res., 2013, 46, 1636-1646.

[28] P. Zhang, Y. Hu, B. Li, Q. Zhang, C. Zhou, H. Yu, X. Zhang, L. Chen, B. Eichhorn, S. Zhou, ACS Catal., 2015, 5, 1335-1343.

[29] J. He, Z. Liu, Y. Yoneyama, N. Nishiyama, N. Tsubaki, Chem. A Eur. J., 2006, 12, 8296-8304.

[30] J. Bao, J. He, Y. Zhang, Y. Yoneyama, N. Tsubaki, Angew. Chem. Int. Ed., 2008, 47, 353-356.

[31] E.G. Derouane, J. Catal., 1986, 100, 541-544.

[32] P. Perez-Uriarte, M. Gamero, A. Ateka, M. Diaz, A.T. Aguayo, J. Bilbao, Ind. Eng. Chem. Res., 2016, 55, 1513-1521.

[33] N. Rahimi, R. Karimzadeh, Appl. Catal. A: Gen., 2011, 398, 1-17.

[34] G. Yang, J. He, Y. Zhang, Y. Yoneyama, Y. Tan, Y. Han, T. Vitidsant, N. Tsubaki, Energy and Fuels, 2008, 22, 1463-1468.

[35] G. Yang, Y. Tan, Y. Han, J. Qiu, N. Tsubaki, Catal. Commun., 2008, 9, 2520-2524.

[36] G. Yang, N. Tsubaki, J. Shamoto, Y. Yoneyama, Y. Zhang, J. Am. Chem. Soc., 2010, 132, 8129-8136.

[37] G. Yang, D. Wang, Y. Yoneyama, Y. Tan, N. Tsubaki, Chem. Commun., 2012, 48, 1263-1265.

[38] G. Yang, M. Thongkam, T. Vitidsant, Y. Yoneyama, Y. Tan, N. Tsubaki, Catal. Today, 2011, 171, 229-235.

[39] K. Fujimoto, Y. Kudo, H. Tominaga, J Catal., 1984, 87, 136-143.

[40] D. Van Vu, M. Miyamoto, N. Nishiyama, S. Ichikawa, Y. Egashita, K. Ueyama, Microporous Mesoporous Mater., 2008, 115, 106-112.

[41] L. Wang, D. Fang, X. Huang, S. Zhang, Y. Qi, Z. Liu, J Nat. Gas Chem., 2016, 15, 38-44.

[42] X. Zhang, P. Zhang, H. Yu, Z. Ma, S. Zhou, Catal. Lett., 2015, 145, 784-793.

[43] R. Q. Long, R. T. Yang, J. Catal., 2001, 198, 20-28.

[44] D. Mores, E. Stavitski, S. P. Verkeleij, A. Lombard, A. Cabiac, L. Rouleau, J. Patarin, A. Simon Masseron, B. M. Weckhuysen, Phys. Chem. Chem. Phys., 2011, 13, 15985-15994.

[45] Q. Lin, Q. Zhang, G. Yang, Q. Chen, J. Li, Q.Wei, Y. Tan, H. Wan, N. Tsubaki, J. Catal., 2016, 344, 378-388.

[46] L. Tan, G. Yang, Y. Yoneyama, Y. Kou, Y. Tan, T. Vitidsant, N. Tsubaki, Appl. Catal A: Gen., 2015, 505, 41-149.

Table 2.1 Physical properties of different samples.

Catalysts	Specific surface area (m^2/g)	Micropore surface area (m^2/g)	Pore volume（ml/g）	Average pore diameter (nm)	Size of PdO (nm)[a]	Amount of surface Pd (atomic %)[b]
SiO_2	294.4	0	1.1	15.3	-	
Pd/SiO_2	230.5	11.3	0.8	14.5	6.7	1.3
Pd/SiO_2-S	241.8	20.5	0.6	17.2	7.0	0.35
Pd/SiO_2-M	233.5	40.5	0.6	17.7	6.9	-
Pd/SiO_2-SZ	248.1	68.5	0.5	19.3	7.1	0

[a] Size of PdO is calculated by Scherrer formula. [b] Amount of surface Pd is determined based on the XPS results.

Table 2.2 Catalysts activity and products distribution over different catalysts.[a]

Catalysts[b]	Conv. (%)		Selectivity (%)								
	CO	CO_2	MeOH	DME	CH_4	C_2H_6	C_3H_8	C_4H_{10}	C_5H_{12}	others[c]	LPG
Pd/SiO_2	14.4	12.7	76.9	3.2	15.3	1.9	1.2	0.6	0.4	0	1.8
Pd/SiO_2-S	12.9	11.8	12.9	24.1	59.8	2.9	0.2	0	0	0	0.2
Pd/SiO_2-M	20.3	10.2	6.9	17.8	39.8	17.2	8.1	5.2	3.1	2.0	13.3
Pd/SiO_2-SZ	14.1	10.7	2.2	2.0	24.3	33.1	27.8	6.7	2.5	1.6	34.4

[a] Reaction conditions：623 K, 5.0 MPa, 4 h, $W_{catalysts}/F_{syngas}$= 10 $g \cdot h \cdot mol^{-1}$, syngas: $H_2/CO/CO_2/Ar$=62.78/29.3/4.95/2.97. [b] Weight of catalysts (core catalyst weight is the same): Pd/SiO_2-0.5 g, Pd/SiO_2-S-0.6 g, Pd/SiO_2-SZ-0.6 g, Pd/SiO_2-M-0.6 g. [c] Others mainly consist of C_6 and C_7 hydrocarbons.

Table 2.3 The effect of reaction temperature on the catalytic performance of Pd/SiO_2-SZ zeolite capsule catalyst for LPG direct synthesis from syngas.[a]

Catalyst[b]	Temp. (K)	Conv. (%)		Selectivity (%)								
		CO	CO_2	MeOH	DME	CH_4	C_2H_6	C_3H_8	C_4H_{10}	C_5H_{12}	others[c]	LPG
Pd/SiO_2-SZ	573	9.0	9.2	11.4	42.5	36.7	5.2	3.1	0.9	0.4	0	4.0
	623	14.1	10.7	2.2	2.0	24.3	33.1	27.8	6.7	2.5	1.6	34.4
	673	15.2	8.5	3.2	1.7	72.9	12.6	6.3	2.0	0.9	0.5	8.3

[a] Reaction conditions: 5.0 MPa, 4 h, $W_{catalysts}/F_{syngas}$= 10 $g \cdot h \cdot mol^{-1}$, syngas: $H_2/CO/CO_2/Ar$=62.78/29.3/4.95/2.97. [b] Catalyst weight: 0.6 g.
[c] Others mainly consist of C_6 and C_7 hydrocarbons.

Table 2.4 The effect of reaction pressure on the catalytic performance of Pd/SiO_2-SZ zeolite capsule catalyst for LPG direct synthesis from syngas.[a]

Catalyst[b]	Press.	Conv. (%)		Selectivity (%)								
	(MPa)	CO	CO_2	MeOH	DME	CH_4	C_2H_6	C_3H_8	C_4H_{10}	C_5H_{12}	others[c]	LPG
	2.0	11.5	11.0	6.3	8.6	35.3	24.8	20.2	4.0	0.9	0	24.2
Pd/SiO_2-SZ	3.0	13.3	11.1	4.0	4.5	32.7	29.8	21.9	4.6	1.6	0.9	26.5
	5.0	14.1	10.7	2.2	2.0	24.3	33.1	27.8	6.7	2.5	1.6	34.4

[a] Reaction conditions： 623 K, 4 h, $W_{catalysts}/F_{syngas}$= 10 $g \cdot h \cdot mol^{-1}$, syngas: $H_2/CO/CO_2/Ar$=62.78/29.3/4.95/2.97; [b] Catalyst weight: 0.6 g.
[c] Others mainly consist of C_6 and C_7 hydrocarbons.

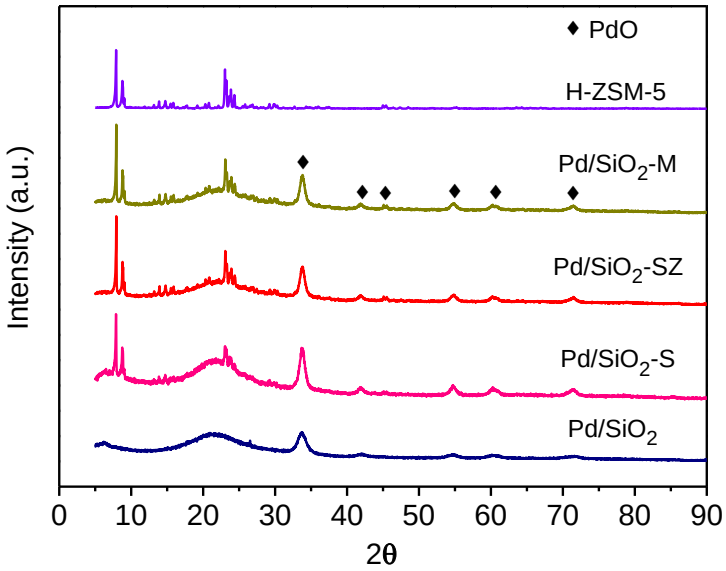

Figure 2.1 XRD patterns of H-ZSM-5 zeolite and different catalysts.

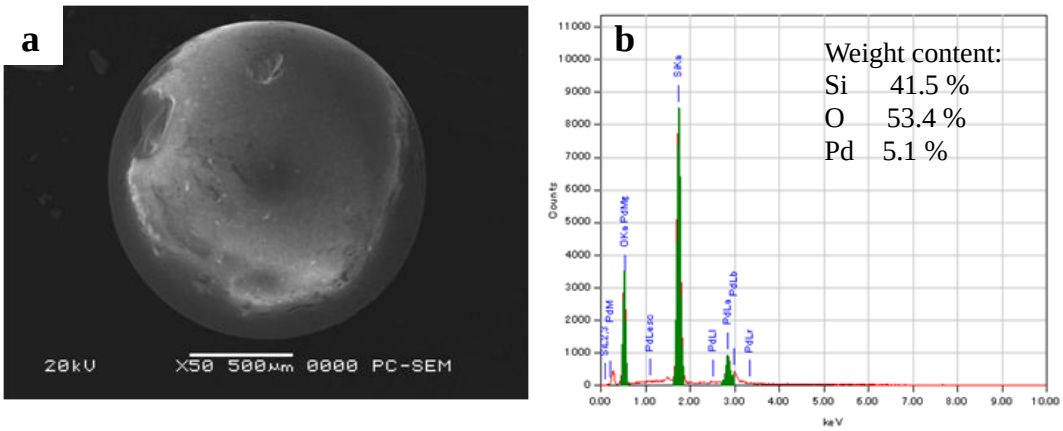

Figure 2.2 (a) Surface SEM image and (b) surface EDS analysis of Pd/SiO_2 catalyst.

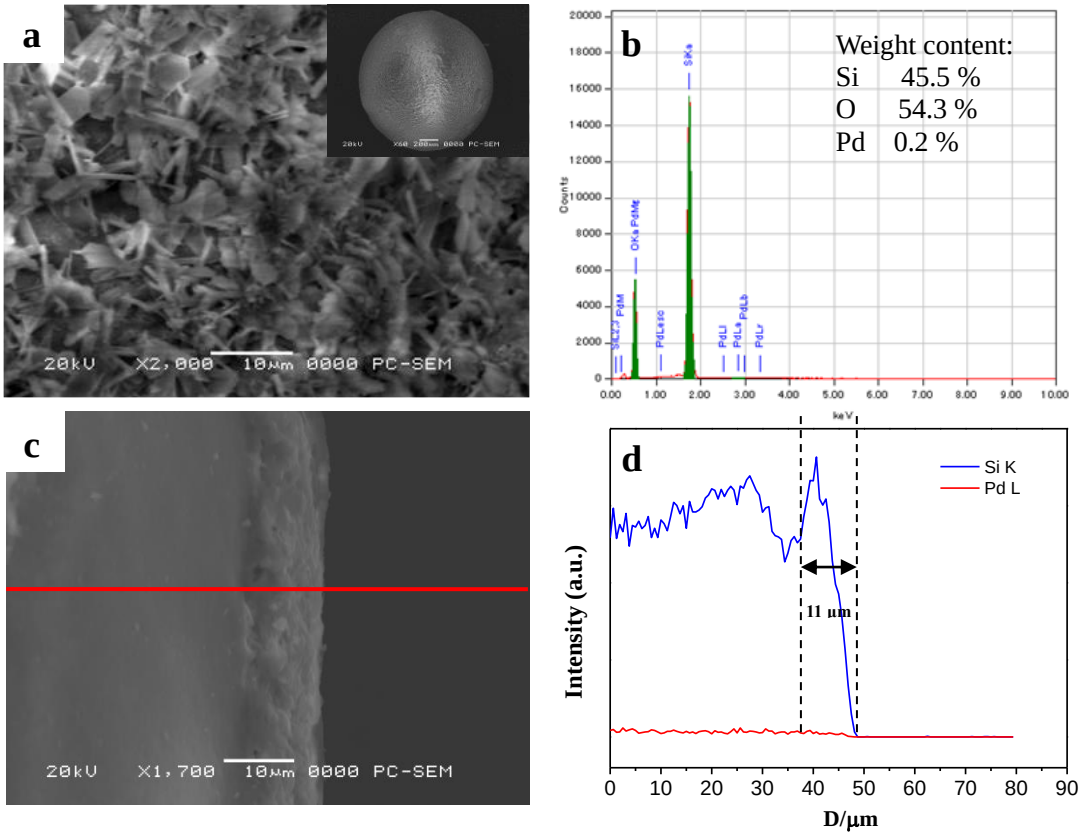

Figure 2.3 The SEM images and EDS line-scanning analysis of Pd/SiO_2-S zeolite capsule catalyst, (a) surface SEM image (inset: complete morphology under lower magnification), (b) surface EDS analysis, (c) cross-section SEM image and (d) EDS line-scan profile.

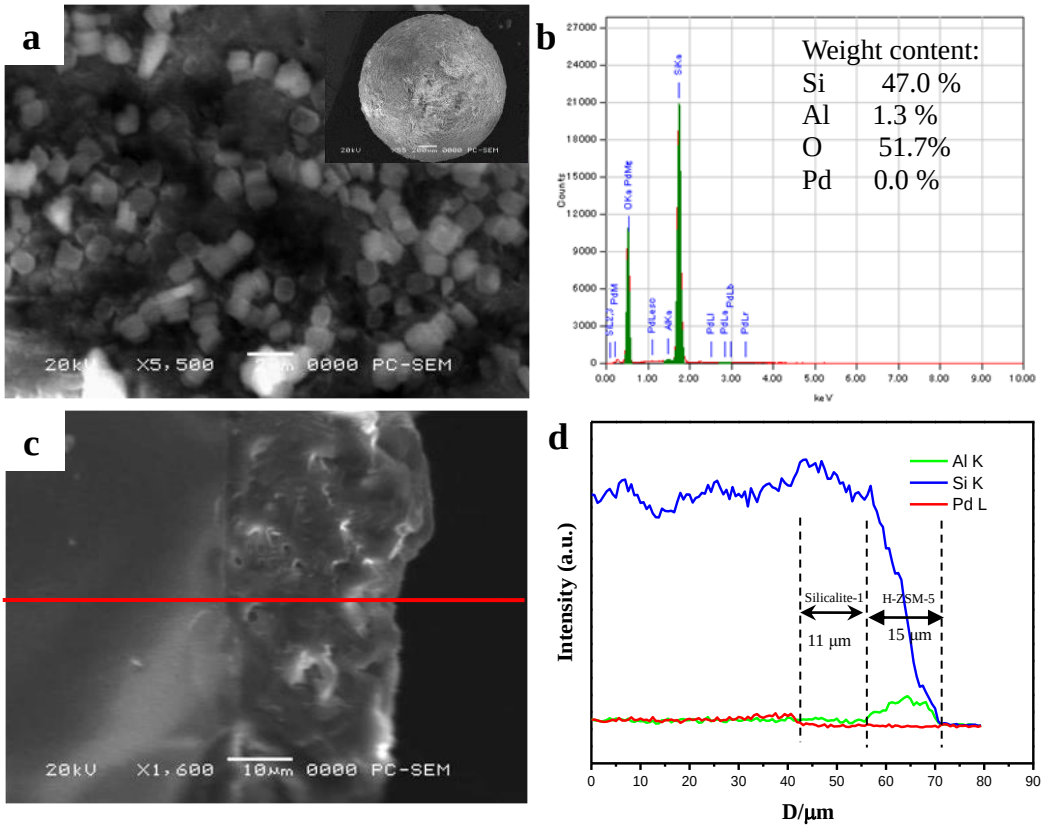

Figure 2.4 The SEM images and EDS line-scanning analysis of Pd/SiO_2-SZ zeolite capsule catalyst, (a) surface SEM image (inset: complete morphology under lower magnification), (b) surface EDS analysis, (c) cross-section image and (d) EDS line-scan profile.

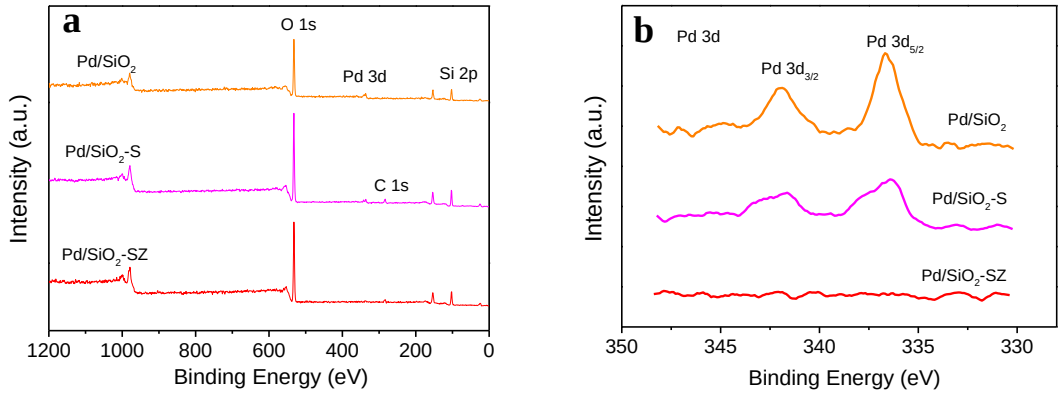

Figure 2.5 The XPS spectra of Pd/SiO_2 core catalyst, Pd/SiO_2-S and Pd/SiO_2-SZ capsule catalysts, (a) XPS survey spectrum, (b) high-resolution Pd 3d.

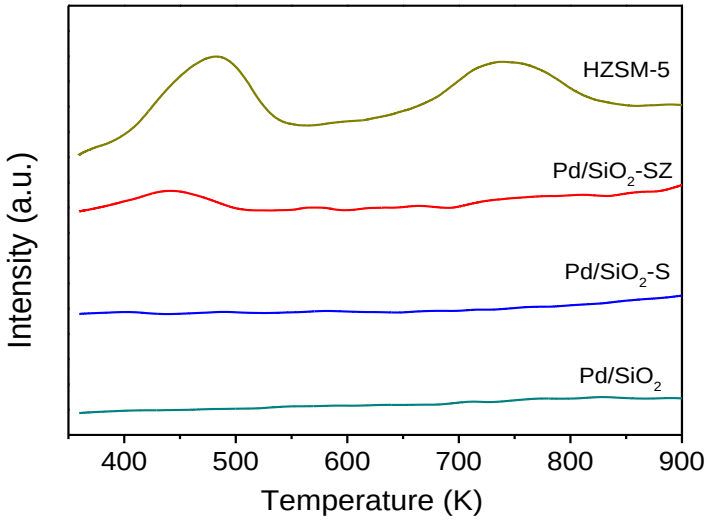

Figure 2.6 The NH_3-TPD profiles of H-ZSM-5 and Pd-based catalysts.

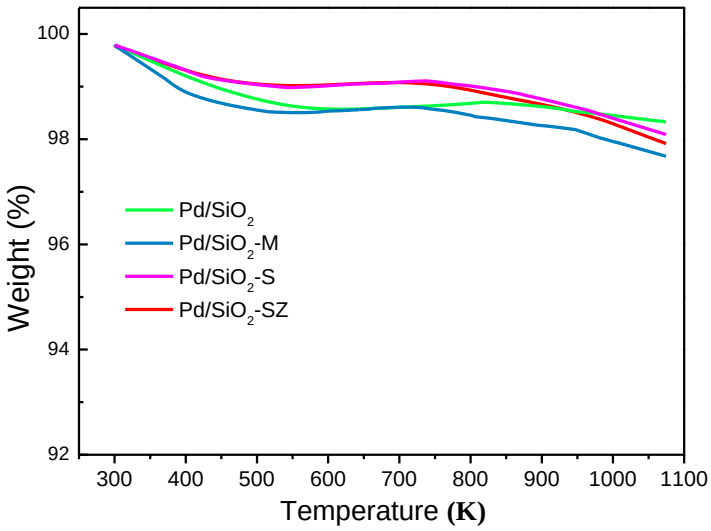

Figure 2.7 The weight loss of all spend catalysts in the LPG synthesis from syngas.

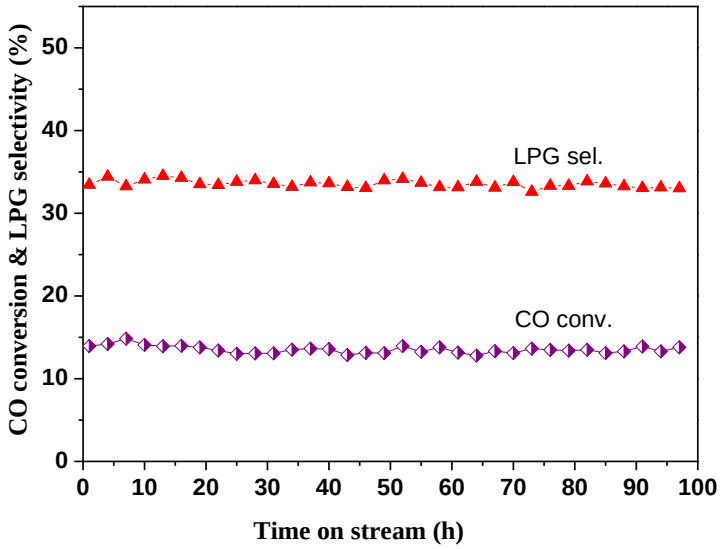

Figure 2.8 The catalytic performance of Pd/SiO_2-SZ zeolite capsule catalyst in the LPG synthesis from syngas as time on stream. Reaction conditions：623 K, 5.0 MPa, $W_{catalysts}/F_{syngas}$= 10 $g \cdot h \cdot mol^{-1}$, syngas: $H_2/CO/CO_2/Ar$=62.78/29.3/4.95/2.97, catalyst weight: 0.6 g.

Chapter 3

One-pass Selective Conversion of Syngas to para-Xylene

We presented a successful hybrid catalyst Cr/Zn-Zn/Z5@S1 for one-pass conversion of syngas to para-xylene with high activity, selectivity, stability and lower CO_2 formation.

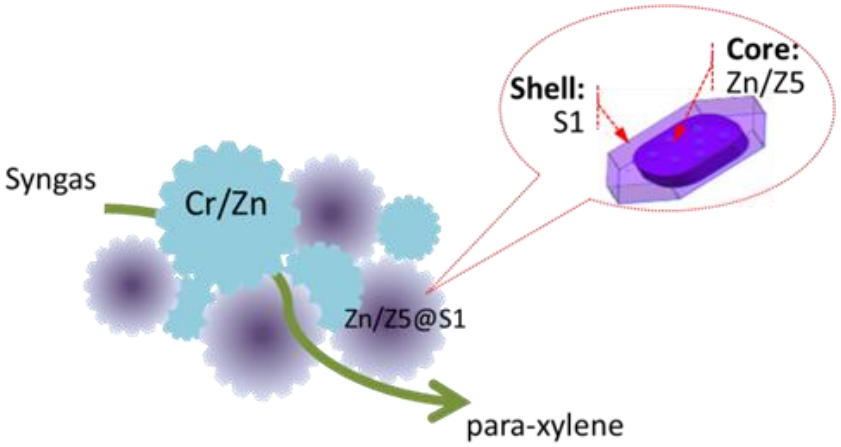

Abstract

The finite petroleum resource and environmental crisis compel the development of non-petroleum carbon resources by chemical transformation routes. Syngas ($CO+H_2$) is a crucial junction point that exclusively bridges the non-petroleum carbon resources and other basic chemicals like alcohols, alkane/alkenes, etc. However, the one-pass conversion of syngas to value-added aromatics, especially para-xylene, is still in a big challenge. Here, we presented a promising hybrid catalyst, named Cr/Zn-Zn/Z5@S1, to effectively realize the one-pass conversion of syngas to para-xylene. This hybrid catalyst exhibited enhanced activity on syngas conversion (CO conversion of 55.0%), good stability on catalyst lifetime and considerable selectivity of para-xylene (27.6% in total products and 77.3% in xylene). The characterization and catalytic performance evaluation revealed that the well-designed core-shell Zn/Z5@S1 zeolite, as a vital part of this Cr/Zn-Zn/Z5@S1 hybrid catalyst, substantially contributed its extreme performance for the para-xylene one-pass precise synthesis from syngas. The concerted combination of two components in this hybrid catalyst can effectively depress the formation of unwanted by-products and facilitate the oriented synthesis of para-xylene from syngas with unprecedented efficiency at the same time.

Keywords: Syngas, para-Xylene, Core-shell zeolite, Aromatic, Xylene

3.1. Introduction

Syngas, a mixture gas of CO and H_2, can be produced from non-petroleum sources, including natural gas, coal and biomass, etc. It is usually used as the raw material to produce other chemicals like dimethyl ether, light olefins, gasoline, diesel, even aromatics through indirect conversion process of Fischer-Tropsch synthesis (FTS)/methanol synthesis and other subsequent catalytic reactions [1-10]. The production of alkane/alkene and aromatic from methanol has received much attention in recent years [11-14]. But the methanol as an intermediate is synthesized separately from syngas through methanol synthesis reaction [15]. To date, one-pass selective conversion of syngas into the target products, like dimethyl ether, isoparaffins/olefins and aromatics has made noticeable progress [16-21], although the catalyst activity and CO_2 formation are still in a challenge. Aromatic hydrocarbon, generally being produced through petroleum industry, is one of the most important basic chemicals. The production of aromatic hydrocarbon from syngas is a crucial alternative process. Among all kinds of aromatic hydrocarbons, para-xylene (PX) is a significant value-added chemical, since it has an important use for producing terephthalic acid (TPA) and other chemicals [22]. The PX is produced by the catalytic reforming of petroleum naphtha as part of the BTX aromatics (benzene, toluene and xylene isomers) [23]. And the separation of PX from aromatics mixture is a high energy-consuming process. Alternative technology for the one-pass synthesis of PX based on a non-petroleum route is required due to the growing demand of PX annually and decreasing reserves of petroleum.

Aromatics synthesis from methanol has been widely studied [24,25]. A higher PX selectivity is always desired in the methanol to aromatics (MTA) reactions [26,27]. H-ZSM-5 zeolite is known for converting methanol to PX because of its channel architecture with suitable size and alterable acidity. Unfortunately, the isomerization of xylene, the main side reaction, simultaneously occurs on the external surface of the H-ZSM-5 zeolite leading to low PX selectivity [26]. Several approaches, such as metal

or metal oxide impregnation, non-acidic silica deposition and so on, have been conducted to passivate the exterior acid sites of H-ZSM-5 to avoid the undesirable xylene isomerization [28-35].

The methanol for MTA reaction must be separately synthesized from syngas. The direct synthesis of aromatics from syngas should be more favourable in view of thermodynamics and economics. However, previous studies on the direct conversion of syngas to alkanes/alkenes only reported the formation of aromatics mixture, never xylene [36,37]. The direct conversion of syngas to aromatics is a complicated process over a typical mixture catalyst. Generally, methanol is first synthesized from syngas over a methanol synthesis catalyst, and then the formed methanol will be converted to aromatics over an acidic zeolite catalyst. Due to the complex reaction paths and harsh reaction conditions, the selectivity of xylene, let alone PX, among the generated aromatics is very low. Designing an efficient route to directly convert syngas into PX is highly required, but it is still in a serious challenge. And until now, there is no report about the one-pass selective conversion of syngas into PX.

In this report, we will present a hybrid catalyst that contains a Cr-based catalyst and core-shell-structured zeolite. With this novel hybrid catalyst, we can facilely realize the one-pass selective conversion of syngas to PX. Typically, the hybrid catalyst, named Cr/Zn-Zn/Z5@S1, is composed of two components: one is Cr/Zn and the other one is a core-shell-structured zeolite Zn/Z5@S1 (zinc doped H-ZSM-5 single crystal zeolite encapsulated with one Silicalite-1 zeolite shell). The Cr/Zn component with a $ZnCr_2O_4$ spinel structure is prepared through a co-precipitation method. The core-shell-structured Zn/Z5@S1 zeolite with a non-acidic Silicalite-1 shell is synthesized through hydrothermal synthesis. All the information about this Cr/Zn-Zn/Z5@S1 hybrid catalyst preparation has been described in detail in the experimental section.

3.2. Experimental section

3.2.1 Catalysts preparation

3.2.1.1 Cr/Zn catalyst preparation

The Cr/Zn catalyst was prepared with the Cr to Zn atomic ratio of 2/1 through a typical co-precipitation method. $Zn(NO_3)_2 \cdot 6H_2O$ and $Cr(NO_3)_3 \cdot 9H_2O$ were first dissolved in deionized water; the above solution and $(NH_4)_2CO_3$ aqueous solution were added dividedly into one beaker by dropwise with constant pH of 7~8 at 343 K under continuous stirring for 1 h, then followed by 3 h aging time at the same temperature. Finally, the obtained mixture was filtered and washed by deionized water, followed by drying in an oven at 393 K overnight and by calcination in air at 773 K for 3 h. The final sample was granulated into a size of 0.85-1.70 mm and denoted as Cr/Zn.

3.2.1.2 H-ZSM-5 (Z5) zeolite preparation

H-ZSM-5 zeolite with different Si/Al ratio (20, 46, 82 and 750) was prepared by hydrothermal synthesis method through adjusting the Si/Al ratios of precursor. The synthesis solution of H-ZSM-5 (2TEOS: 0.68TPAOH: 8EtOH: $120H_2O$: xAl_2O_3, x=0.001-0.05) was enclosed in an autoclave and heated to 453 K for 24 h with a rotation rate of 2 r/min. After crystallization, the samples were separated from mother solution and washed by deionized water for several times until the pH=7, then followed by drying at 393 K for 12 h. Finally, the H-ZSM-5 zeolite was obtained after calcination at 823 K for 6 h with heating rate of 1 K/min, and denoted as Z5 in this paper.

3.2.1.3 The Zn/Z5 catalyst preparation

The obtained Z5 (Si/Al=46) sample was modified by Zn through ion-exchange method. Briefly, 1.5 g Z5 powder was added to 0.1 M $Zn(NO_3)_2$ aqueous solution at 353 K with continuously stirring for 15 h. After stirring, the obtained powder was washed by deionized water for three times, followed by drying at 393 K and calcination at 823 K for 5 h. The prepared sample was denoted as Zn/Z5.

3.2.1.4 The preparation of core-shell-structured Zn/Z5@S1 and Z5@S1 zeolite

The epitaxial crystal growth of Zn/Z5 (Si/Al=46) or Z5 (Si/Al=46) was performed

through hydrothermal synthesis in the mother liquid for Silicalite-1 zeolite growth. 1.0 g Zn/Z5 or Z5 powder was added to the zeolite synthesis solution with the recipe of 1.00SiO_2: 0.06TPAOH: 16.0EtOH: 240H_2O. Then the mixture was moved into a teflon-lined autoclave for zeolite crystal epitaxial growth at 453 K for 24 h with a rotation rate of 3 r/min. The sample collection process is similar to that of Z5 sample. The above Silicalite-1 shell coating process was conducted twice. The obtained samples were named as Zn/Z5@S1 and Z5@S1, respectively.

3.2.1.5 The hybrid catalysts preparation

All the hybrid catalysts were prepared by physically mixing the two components of Cr/Zn and Z5-based zeolite, followed by grinding and granulating into the required size in the range of 0.85-1.70 mm. In order to investigate the effect of Si/Al ratio of Z5 on the hybrid catalyst performance, we first prepared a series of simplest hybrid catalyst Cr/Zn-Z5 with different Z5 (Si/Al=20, 46, 82 and 750) as the zeolite components. The Z5 zeolite (Si/Al=46) derived zeolite components, Zn/Z5, Z5@S1 and Zn/Z5@S1, were used for the preparation of hybrid catalysts Cr/Zn-Zn/Z5, Cr/Zn-Z5@S1 and Cr/Zn-Zn/Z5@S1.

3.2.1.6 The dual-layer catalyst model in reactor

As the reference of hybrid catalysts, the dual-layer catalyst model that was composed of top Cr/Zn layer and bottom Zn/Z5@S1 layer, named Cr/Zn+Zn/Z5@S1 (dual-layer), in the reactor had also been evaluated under the same reaction conditions. The Cr/Zn and Zn/Z5@S1 components were pelleted into the size of 0.85-1.70 mm respectively in advance.

3.2.1.7 The granule mixture catalyst model in reactor

As another reference catalyst of hybrid catalyst, the granular mixture catalyst model prepared by simply mixing granular Cr/Zn (0.8-1.70 mm) and granular Zn/Z5@S1 (0.8-1.7mm) had also been evaluated under the same reaction conditions. It was called

Cr/Zn+Zn/Z5@S1 (granule mixture) in the followed discussion.

3.2.2 Catalysts characterization

The crystal structures of catalysts were determined by powder X-ray diffraction patterns (XRD), which were performed at Rigaku RINT 2400 X-ray Diffractometer equipped with a Cu Kα radiation. Scans were recorded in the 2θ range 5-90° with a step size of 0.02 °/s. The physical properties of catalysts, such as surface area, microspore volume and average pore size, were analyzed by N_2 physical adsorption at 77 K. These data were measured using Micrsmertics 3Flex specific surface area and porous physical adsorption analyzer. All samples were degassed in vacuum at 473 K for 5 h before measurement.

The scanning transmission electron microscopy images (STEM) and transmission electron microscopy images (TEM) were performed on a JEM-2100F (JEOL) at an acceleration voltage of 200 kV. The surface morphology and elemental composition were obtained by field-emission scanning electron microscope (FE-SEM, JEOL JSM-6700F) and scanning electron microscope (SEM, JEOL JSM-6360LV) with JED-2300 energy dispersive spectroscopy (EDS) attachment. The samples were per-treated in vacuum at 343 K overnight and sprayed platinum at 10 kv for 200 s before examination.

The X-ray photoelectron spectroscopy (XPS) analysis was done by Thermo Fisher Scientific ESCALAB 250Xi multifunctional X-ray photoelectron spectroscope, by which to determine the existence of Al and Zn on the outward appearance of catalysts. The data processing was performed using Avantage software. The inductive coupled plasma atomic emission spectrometry (ICP-AES) was employed to determine the real Zn content of zeolite materials using Perkin Elmer Optima 7300DV atomic emission spectrometry spectrometer.

NH_3 temperature programmed desorption (NH_3-TPD) was conducted by a catalyst analyzer BELCAT-B-TT (BEL Japan Co. Ltd.) equipped with a thermal conductivity

detector (TCD). 0.03 g sample was pretreated at 423 K in He flow for 1 h, then 5% NH_3 in He was introduced for 1 h with flow rate of 20 ml/min while temperature was cooling down to 353 K. Subsequently, the microreactor was purified with pure He for 1 h. Finally, the NH_3 desorption procedure was proceeded in He flow (30 ml/min) by increasing the temperature from room temperature to 1073 K with a ramping rate of 5 K/min. The density of acid sites was quantified by peak area of the high-temperature NH_3-desorption peaks.

Thermogravimetry (TG) measurement was carried out over 10 mg spent catalysts in air with flow rate of 30 ml/min using TA-60WS thermal analyzer (Shimadzu). The program was performed at the heating rate of 10 K/min from room temperature to 1173 K.

3.2.3 Catalysts evaluation

The catalyst performance evaluation of catalysts for PX direct synthesis from syngas was carried out in a fixed-bed steel reactor with internal diameter of 6 mm. All of catalysts were first reduced in the reactor for 10 h at 673 K with pure H_2. After cooling down to the room temperature, syngas with H_2/CO molar ratio of 2 was introduced into the reactor. Then, the reaction was conducted at 673 K under 5.0 MPa. All the products were kept in the gas phase from reactor to outlet and analyzed by an on-line gas chromatograph (GC-8A, Shimadzu), which was equipped with Plot S columns for the thermal conductivity detector (TCD), and HP-PLOT/Q columns for the flame ionization detector (FID). The CO conversion and the hydrocarbons selectivity were calculated with the followed equations, using Ar as an inner standard.

$$C_{CO}=(X_{CO,\,in} - X_{CO,\,out})/ (X_{CO,\,in}) \times 100\% \quad (3\text{-}1)$$

C_{CO}: Conversion of CO, %; $X_{CO,\,in}$: Mole fraction of CO in pristine syngas;

$X_{CO,\,out}$: Mole fraction of CO in exit gas;

$$C_{CO2}=(X_{CO2,\,in} - X_{CO2,\,out})/ (X_{CO2,\,in}) \times 100\% \quad (3\text{-}2)$$

C_{CO2}: Conversion of CO_2, %; $X_{CO2,\ in}$: Mole fraction of CO_2 in pristine syngas;

$X_{CO2,\ out}$: Mole fraction of CO_2 in exit gas;

$$\mathbf{Sel_i} = \frac{\mathbf{R_{i,s}f_{i,m}}}{\sum_{\mathbf{i}}\mathbf{R_{i,s}f_{i,m}}} \tag{3-3}$$

Sel_i: Mass selectivity of component i, %; $f_{i,\ m}$: Factor of mass correction;

$R_{i,\ s}$: Area ratio of hydrocarbon in chromatogram.

$$\mathbf{PX/X} = \frac{\mathbf{Sel_{PX}}}{\mathbf{Sel_{OX}} + \mathbf{Sel_{MX}} + \mathbf{Sel_{PX}}} \times 100\% \tag{3-4}$$

$\mathbf{PX/X}$: Selectivity of para-xylene in total xylene isomers;

$\mathbf{Sel_{OX}}$: Selectivity of ortho-xylene; $\mathbf{Sel_{MX}}$: Selectivity of meta-xylene;

$\mathbf{Sel_{PX}}$: Selectivity of para-xylene.

3.3. Results and discussion

3.3.1 Structure and surface properties of catalysts

The detailed physical properties of the Cr/Zn component are characterized by XRD, (Figure 3.1). The analysis results indicate that the $ZnCr_2O_4$ spinel is successfully synthesized on the Cr/Zn component. The physical morphology and element composition of Cr/Zn catalyst were determined by SEM-EDS. Figure 3.2 presented the SEM and EDS analysis results, in which the molar ratio of Cr/Zn is 2.04. The synthesis procedure for the core-shell-structured Z5@S1 and Zn/Z5@S1 zeolite components is shown in Scheme 3.1. The detailed preparation methods of these zeolite components are also described in the experimental section. The original Z5 (H-ZSM-5, Si/Al=46) or Zn/Z5 (Zn doped Z5, 1.0 wt% by ICP analysis) is used as the zeolite core for the core-shell-structured Z5@S1 and Zn/Z5@S1 zeolite synthesis, respectively, by epitaxially growing Silicalite-1 shell on the zeolite cores. The XRD profiles of all the zeolite components used for hybrid catalyst preparation are also shown in Figure 3.1. The classic peaks of MFI zeolite appear in the ranges of 2θ=7-10° and 22-26°,

indicating that the MFI structure of Z5 zeolite is stable after the modification by Zn and the encapsulation with Silicalite-1 zeolite shell [38]. And no peaks belonging to Zn species are discovered on the Zn/Z5 and Zn/Z5@S1 zeolite because the amount of Zn on these samples is too low to be detected.

We employ SEM to characterize all the zeolite components and the results are shown in Figure 3.3. The SEM image of pure Z5 is showed in Figure 3.3a. The Zn doped Z5 zeolite will not affect the original zeolite morphology, as presented by Zn/Z5 sample in Figure 3.3c. With Z5 or Zn/Z5 as the mother zeolite, we epitaxially grow their body through hydrothermal synthesis process in the synthesis solution for Silicalite-1 zeolite growth, in order to get the Silicalite-1 shell encapsulated zeolite Z5@S1 and Zn/Z5@S1. The surface morphology of the typical Zn/Z5 and Zn/Z5@S1 zeolite measured by FE-SEM is also given in Figure 3.4a and 3.4b. For the core-shell-structured Zn/Z5@S1 zeolite, as shown in Figure 3.4b, the Zn/Z5 core zeolite has been fully encapsulated by Silicalite-1 zeolite layer. The Zn/Z5@S1 sample has a hexagon exterior shape with particle length of around 2.5μm. The original Zn/Z5 core zeolite has a rounded hexagon shape with the smaller size of around 1μm (Figure 3.4a). The epitaxial growth of the Silicalite-1 shell is along the outside surface of Z5 crystal [15, 34]. The STEM and EDS mapping analysis on the core-shell-structured Zn/Z5@S1 zeolite are given in Figure 3.4c-3.4h. The Al and Zn elements distribute mainly inside the white circle, indicating the Zn/Z5 core section of Zn/Z5@S1 zeolite. Moreover, the XPS analysis also shows that the number of Zn and Al species is zero in the near-surface regions of the Zn/Z5@S1 zeolite (Figure 3.5 and Table 3.1). The physical properties of all the Cr/Zn component and zeolite components are also summarized in Table 3.2 and Figure 3.6. As presented in Table 3.2, Cr/Zn catalyst illustrates BET surface area of 98.9 m^2/g, pore volume of 0.58 cm^3/g and 21.5 nm averaged pore size. The BET surface area, pore volume and average pore size of hybrid catalysts are similar because of the same ratio of Cr/Zn and approximate textural properties of Z5-based

zeolite materials. All the analysis results prove that the prepared Zn/Z5@S1 zeolite possesses an ideal core-shell structure, in which the Zn/Z5 zeolite core is entirely enwrapped by Silicalite-1 zeolite shell.

The acidity of all zeolite components for hybrid catalysts preparation was evaluated by NH_3-TPD, and the results are shown in Table 3.3 and 3.4, and in Figure 3.7 and 3.8. The NH_3-TPD profiles of H-ZSM-5 with different Si/Al ratio are displayed in the Figure 3.7. The NH_3 desorption peak areas of weak and strong acid sites decrease with increasing the Si/Al ratio. It is consistent with the acidic sites from the calculation, as presented in Table 3.3. The type of acidic sites for Z5 and Zn/Z5 are similar, while the acidic concentration of Zn/Z5 is less than that of Z5; because few Al atoms in Z5 are replaced by Zn. The core-shell-structured Z5@S1 and Zn/Z5@S1 have a lower acidic strength and acidic concentration than those of Z5 and Zn/Z5, indicating that the introduced Silicalite-1 shell neutralizes and seals the surface acidic sites of Z5 (Figure 3.8 and Table 3.4). The designed Silicalite-1 shell will effectively seal the surface acidic sites of core zeolite, whereby to depress the formation of ortho-, meta-xylene, at the same time boosting the generation of PX in the followed reaction [27, 39].

3.3.2 Catalytic performance of varied catalysts for PX synthesis

By physically mixing the Cr/Zn component and zeolite components (Z5, Zn/Z5, Z5@S1 and Zn/Z5@S1), we get a series of hybrid catalysts Cr/Zn-Z5, Cr/Zn-Zn/Z5, Cr/Zn-Z5@S1 and Cr/Zn-Zn/Z5@S1. The effect of a varied Si/Al ratio (20, 46, 82 and 750) of Z5 in the simplest hybrid catalyst Cr/Zn-Z5 for PX one-pass synthesis from syngas is investigated, as shown in Figure 3.9 and Table 3.5. It is clear that the most suitable Si/Al ratio of Z5 is around 46. Therefore, the followed hybrid catalysts are prepared with the Z5 (Si/Al=46) as the zeolite component.

All of the hybrid catalysts are evaluated to investigate their catalytic performance for the one-pass PX synthesis from syngas, and the reaction results are compared in Table 3.6. The catalytic reaction is conducted under a pressure of 5.0 MPa and a

temperature of 673 K. The single Cr/Zn catalyst, as reference catalyst, is also tested under the same reaction conditions. The CO conversion over the Cr/Zn catalyst is 27.5% with the major products of MeOH, DME and CH_4. In contrast, all of the hybrid catalysts present higher CO conversion and zero formation of methanol and DME. The introduced zeolite components in the hybrid catalysts promote the CO conversion by shifting the thermodynamics equilibrium of MeOH synthesis. In addition to the enhanced CO conversion, all of the hybrid catalysts can convert syngas directly into alkane/alkenes and xylene. As given in Table 3.6, the Cr/Zn-Zn/Z5@S1 hybrid catalyst shows excellent xylene selectivity of 35.7%, in which the selectivity of PX reaches up to 27.6%. The PX selectivity in the total xylene is 77.3%, the highest value among all the tested catalysts.

From the view point of diffusion, the distance between the components of Cr/Zn and Zn/Z5@S1 is considerably crucial for hybrid catalyst. Other components assembly model of Cr/Zn+Zn/Z5@S1 (dual-layer) and Cr/Zn+Zn/Z5@S1 (granule mixture), as the references of Cr/Zn-Zn/Z5@S1 hybrid catalyst were also designed and evaluated (Table 3.6 and Figure 3.10). The Cr/Zn+Zn/Z5@S1 (dual-layer) comprises a top Cr/Zn layer and a bottom Zn/Z5@S1 layer in one reactor (Figure 3.10b). The formed MeOH and DME in the top Cr/Zn layer are largely converted into alkanes/alkenes (C_2-C_5=59.1%), but little PX (2.1%). Methane formation (26.8%) cannot be inhibited, because of the long distance between Cr/Zn and Zn/Z5@S1. The Cr/Zn+Zn/Z5@S1 (granule mixture) can further decrease the distance between Cr/Zn and Zn/Z5@S1 (Figure 3.10c). The CO conversion is promoted up to 50.4%, obviously higher than that of the single Cr/Zn and Cr/Zn+Zn/Z5@S1 (dual-layer). Methane selectivity is only 7.2%. But alkanes/alkenes (C_2-C_5=66.6%) existed still, with a low PX selectivity of 5.2%. In contrast, the Cr/Zn-Zn/Z5@S1 hybrid catalyst, prepared by milling two components powder adequately, ensures the shortest distance between components in hybrid catalyst (Figure 3.10d). As a result, we got the highest CO conversion (55.0%),

the highest PX (27.6%) selectivity, at the same time as a lower selectivity of CH_4 and C_2-C_5, as given in Table 3.6. The two components in the hybrid catalyst are close to each other. The formed intermediates can diffuse quickly to the Zn/Z5@S1 component, and are converted into PX. Besides, rapidly removing the intermediates from the Cr/Zn component can push the thermodynamic equilibrium to shift towards methanol synthesis from syngas, therefore depressing other competitive side reactions like methanation, etc. The comparison of the three catalyst models, Cr/Zn-Zn/Z5@S1 hybrid catalyst, Cr/Zn+Zn/Z5@S1 (granule mixture) and Cr/Zn+Zn/Z5@S1 (dual-layer), proves that a short distance between two components is required for the design of hybrid catalyst to realize PX selective synthesis directly from syngas.

The selectivity of xylene and PX over the hybrid catalysts is also compared in Figure 3.11. Both of the highest selectivities on xylene (35.7%) and PX (27.6%) were successfully realized on the Cr/Zn-Zn/Z5@S1 hybrid catalyst. The formation of meta-xylene has been completely suppressed, and the major by-product in xylene isomers is only ortho-xylene. The time on stream of xylene and PX selectivity in the xylene isomers is shown in Figure 3.12. The Cr/Zn-Zn/Z5@S1 hybrid catalyst demonstrates enhanced selectivity and excellent stability for PX synthesis during total reaction time. As indicated by the TEM image in Figure 3.13a, the Cr/Zn-Zn/Z5@S1 hybrid catalyst is composed of a Cr/Zn component and a core-shell-structured Zn/Z5@S1 zeolite component. In the reaction (as illustrated by Figure 3.13b), syngas is first converted into methanol on the Cr/Zn component, and then the formed methanol in-situ undergoes a series of reaction steps like dehydration, C-C bonds coupling, etc., to generate PX over the core-shell-structured Zn/Z5@S1 zeolite component. The two components in this Cr/Zn-Zn/Z5@S1 hybrid catalyst contact tightly, cooperate concertedly and promote mutually. The highest PX selectivity among the products obtained by the Cr/Zn-Zn/Z5@S1 hybrid catalyst should be attributed to its zeolite component of Zn/Z5@S1 with a special core-shell structure. The ion-exchange of Z5

zeolite with Zn generates Lewis acid sites replacing the previous strong acid sites, hence the aromatics selectivity of the hybrid catalysts is clearly improved [40]. The Silicalite-1 shell can seal the exposed external acidic sites of the Zn/Z5 core zeolite, by which to depress the xylene isomerization. As a result, the Cr/Zn-Zn/Z5@S1 hybrid catalyst successfully converts syngas into PX with extremely higher selectivity.

Carbon deposition on the zeolite catalyst is the major factor that will affect the catalyst's life time and performance. TG is employed to measure the carbonaceous species deposited on the spent hybrid catalysts (after 10 h reaction) and the result is given in Figure 3.14. The coke deposition rate of Cr/Zn-Zn/Z5@S1 is in last place among all the catalysts. The coke formation on the zeolite catalyst is initiated at the edge of straight pores in contact with the crystal outer surface [41]. However, for the Cr/Zn-Zn/Z5@S1 hybrid catalyst, Silicalite-1 shell is epitaxially synthesized at the surface of the Zn/Z5 zeolite, which leads to a direct pore to pore connection between Z5 and Silicalite-1 during the hydrothermal synthesis process [42,43]. Therefore, it is demonstrated that the coke formation on the Cr/Zn-Zn/Z5@S1 hybrid catalyst is effectively depressed, ensuring its substantial stability among all the tested catalysts.

3.3.3 Discussion

For the perspective on further enhancing of the xylene yield and para-xylene selectivity, it is practical to tune syngas composition and/or the thickness of Silicalite-1 zeolite shell enwrapping on the single-crystal Zn/Z5 core zeolite of the hybrid catalyst, in order to further depress the formation of alkane/alkenes and other aromatic by-products. Furthermore, precisely controlling the crystal size or channel properties of the Zn/Z5 core zeolite can further enhance the para-xylene selectivity. At the present stage, meta-xylene formation has been completely stopped. Considering the similar kinetic diameter of ortho-xylene and meta-xylene, which are larger than that of para-xylene, further modifying the channels and adjusting the crystal size of the Zn/Z5 core zeolite should be effective tools to tune the intracrystalline diffusivity of products,

therefore erasing the formation of ortho-xylene, and simultaneously lowering the selectivities of other hydrocarbon by-products.

3.4. Conclusions

In summary, we presented a successful hybrid catalyst Cr/Zn-Zn/Z5@S1 for the one-pass conversion of syngas to para-xylene with high activity, selectivity, stability and lower CO_2 formation. The selectivity of PX obtained by this hybrid catalyst reached up to 77.3% in the xylene isomers and accounted for 27.6% of the total hydrocarbons products at the CO conversion of 55.0%. This hybrid catalyst contained two components: one was Cr/Zn and the other one was a core-shell-structured Zn/Z5@S1 zeolite. The combination of two components in this hybrid catalyst enabled performed a well-organized tandem catalysis process, performing syngas to methanol and methanol to PX exclusively. The special core-shell structure of Zn/Z5@S1 could effectively seal the exposed active sites of zeolite, in order to depress the formation of unwanted xylene isomers and promote the oriented synthesis of PX. The hybrid catalyst Cr/Zn-Zn/Z5@S1 reported in this paper is extremely promising as an industrial catalyst, not only for PX synthesis, but also for the direct conversion of syngas to value-added chemicals,

References

[1] M. Cai, A. Palcic, V. Subramanian, S. Moldovan, O. Ersen, V. Valtchev, V.V. Ordomsky, A.Y. Khodakov, J. Catal., 2016, 338, 227-238.

[2] G. Yang, N. Tsubaki, J. Shamoto, Y. Yoneyama, Y. Zhang, J. Am. Chem. Soc., 2010, 132, 8129-8136.

[3] F. Jiao, J. Li, X. Pan, J. Xiao, H. Li, H. Ma, M. Wei, Y. Pan, Z. Zhou, M. Li, S. Miao, J. Li, Y. Zhu, D. Xiao, T. He, J. Yang, F. Qi, Q. Fu, X. Bao, Science, 2016, 351, 1065-1068.

[4] L. Zhong, F. Yu, Y. An, Y. Zhao, Y. Sun, Z. Li, T. Lin, Y. Lin, X. Qi, Y. Dai, L. Gu, J. Hu, S. Jin, Q. Shen, H. Wang, Nature, 2016, 538, 84-87.

[5] H. M. T. Galvis, J. H. Bitter, C. B. Khare, M. Ruitenbeek, A. I. Dugulan, K. P. de Jong, Science, 2012, 335, 835-838.

[6] P. Zhai, C. Xu, R. Gao, X. Liu, M. Li, W. Li, X. Fu, C. Jia, J. Xie, M. Zhao, X. Wang, Y. Li, Q. Zhang, X. Wen, D. Ma, Angew. Chem. Int. Ed., 2016, 55, 9902-9907.

[7] K. Cheng, L. Zhang, J. Kang, X. Peng, Q. Zhang, Y. Wang, Chem. Eur. J., 2015, 21, 1928-1937.

[8] X. Peng, K. Cheng, J. Kang, B. Gu, X. Yu, Q. Zhang, Y. Wang, Angew. Chem. Int. Ed., 2015, 54, 4553-4556.

[9] Q. Zhang, Y. Tan, C. Yang, H. Xie, Y. Han, J. Ind. Eng. Chem., 2013, 19, 975-980.

[10] N. Guan, Y. Liu, M. Zhang, Catal. Today, 1996, 30, 207-213.

[11] U.Olsbye, S. Svelle, M. Bjørgen, P. Beato, T. V. W. Janssens, F. Joensen, S. Bordiga, K. P. Lillerud, Angew. Chem. Int. Ed., 2012, 51, 5810-5831.

[12] S. Bao, L. Tau, B. Davis, J. Catal., 1988, 111, 436-439.

[13] R. Khare, Z. Liu, Y. Han, A. Bhan, J. Catal., 2017, 348, 300-305.

[14] S. Ilias, A. Bhan, ACS Catal., 2013, 3, 18-31.

[15] U. Olsbye, Angew. Chem. Int. Ed., 2016, 55, 7294-7295.

[16] C. D. Chang, W. H. Lang, A. J. Silvestri, J. Catal., 1979, 56, 268-273.

[17] J. Bao, J. He, Y. Zhang, Y. Yoneyama, N. Tsubaki, Angew. Chem. Int. Ed., 2008, 47, 353-356.

[18] H. Seki, N. Tsubaki, Y. Yoneyama, Japan Patent 5517681, 2014.

[19] K. Cheng, B. Gu, X. Liu, J. Kang, Q. Zhang, Y. Wang, Angew. Chem. Int. Ed., 2016, 55, 4725-4728.

[20] B. Zhao, P. Zhai, P. Wang, J. Li, T. Li, M. Peng, M. Zhao, G. Hu, Y. Yang, Y. W. Li, Q. Zhang, W. Fan, D. Ma, Chem, 2017, 3, 323-333.

[21] K. Cheng, W. Zhou, J. Kang, S. He, S. Shi, Q. Zhang, Y. Pan, W. Wen, Y. Wang, Chem, 2017, 3, 334-347.

[22] J. Breen, R. Burch, M. Kulkarni, P. Collier, S. Golunski, J. Am. Chem. Soc., 2005, 127, 5020-5021.

[23] T. W. Lyons, D. Guironnet, M. Findlater, M. Brookhart, J. Am. Chem. Soc., 2012, 134, 15708-15711.

[24] K. Wang, M. Dong, J. Li, P. Liu, K. Zhang, J. Wang, W. Fan, Catal. Sci. Technol., 2017, 7, 560-564.

[25] Z. Wei, L. Chen, Q. Cao, Z. Wen, Z. Zhou, Y. Xu, X. Zhu, Fuel Process. Technol., 2017, 162, 66-77.

[26] J. Zhang, W. Qian, C. Kong, F. Wei, ACS Catal., 2015, 5, 2982-2988.

[27] K. Miyake, Y. Hirota, K. Ono, Y. Uchida, S. Tanaka, N. Nishiyama, J. Catal., 2016, 342, 63-66.

[28] Y. Zhao, H. Wu, W. Tan, M. Zhang, M. Liu, C. Song, X. Wang, X. Guo, Catal. Today, 2010, 156, 69-73.

[29] T. Hibino, M. Niwa, Y. Murakami, J. Catal., 1991, 128, 551-558.

[30] Y. Zhao, W. Tan, H. Wu, A. Zhang, M. Liu, G. Li, X. Wang, C. Song, X. Guo, Catal. Today, 2011, 160, 179-183.

[31] J. H. Ahn, R. Kolvenbach, S. S. Al-Khattaf, A. Jentys, J. A. Lercher, Chem. Commun., 2013, 49, 10584-10586.

[32] J. Li, K. Tong, Z. Xi, Y. Yuan, Z. Hu, Z. Zhu, Catal. Sci. Technol., 2016, 6, 4802-4813.

[33] M. Miyamoto, T. Kamei, N. Nishiyama, Y. Egashira, K. Ueyama, Adv. Mater., 2005, 17, 1985-1988.

[34] F. Wang, W. Xiao, L. Gao, G. Xiao, Catal. Sci. Technol., 2016, 6, 3074-3086.

[35] L. J. Lobree, I. C. Hwang, J. A. Reimer, A. T. Bell, J. Catal., 1999, 186, 242-253.

[36] F. Simard, U. A. Sedran, J. Sepulveda, N. S. Figoli, H. I. de Lasa, Appl. Catal. A: Gen., 1995, 125, 81-98.

[37] J. Ereña, J. M. Arandes, J. Bilbao, A. T. Aguayo, H. I. de Lasa, Ind. Eng. Chem. Res., 1998, 37, 1211-1219.

[38] Y. Peng, Z. Zhan, L. Shan, X. Li, Z. Wang, Y. Yan, J. Membrane Sci., 2013, 444, 60-69.

[39] A. Ghorbanpour, A. Gumidyala, L. C. Lars C. Grabow, S. P. Crossley, J. D. Rimer, ACS Nano, 2015, 9, 4006-4016.

[40] J. A. Biscardi, G. D. Meitzner, E. Iglesia, J. Catal., 1998, 179, 192-202.

[41] D. Mores, E. Stavitski, M. H. F. Kox, J. Kornatowski, U. Olsbye, B. M. Weckhuysen, Chem. Eur. J., 2008, 14, 11320-11327.

[42] D. Van Vu, M. Miyamoto, N. Nishiyama, S. Ichikawa, Y. Egashira, K. Ueyama, Microporous Mesoporous Mater., 2008, 115, 106-112.

[43] D. Mores, E. Stavitski, S. P. Verkleij, A. Lombard, A. Cabiac, L. Rouleau, J. Patarin, A. S. Masseron, B. M. Weckhuysen, Phys. Chem. Chem. Phys., 2011, 13, 15985-15994.

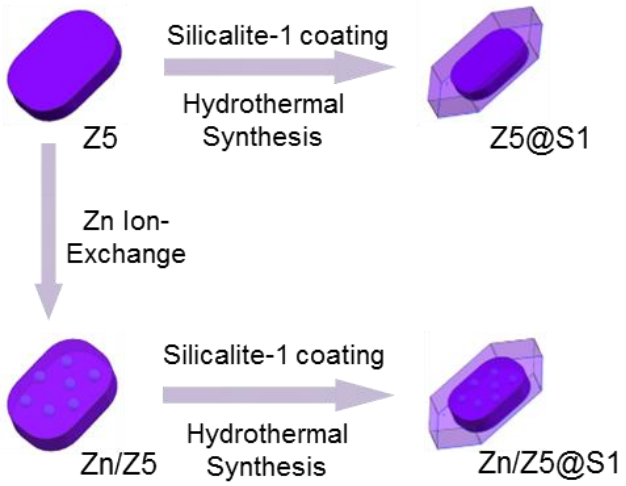

Scheme 3.1 Illustration on the synthesis of the Zn/Z5 and the typical core-shell-structured Z5@S1 and Zn/Z5@S1 zeolite with Z5 (Si/Al=46) as based zeolite.

Table 3.1 The atom amount of Si, Al, Zn and the atom ratio of Si/Al, Zn/Al on the zeolite components obtained from the XPS analysis results

Samples	Si	Al	Zn	Si/Al	Zn/Al
Z5	30.6	0.21	-	145.7	-
Zn/Z5	27.6	0.17	0.08	162.4	0.47
Z5@S1	36.6	0	-	-	-
Zn/Z5@S1	29.2	0	0	-	-

Table 3.2 BET surface area, pore volume and average pore size of samples.

Catalysts	S_{BET} (m^2g^{-1})	Pore volume (cm^3g^{-1})	Average pore size (nm)
Cr/Zn	98.9	0.58	21.5
Cr/Zn-Z5	188.4	0.26	5.8
Cr/Zn-Zn/Z5	190.8	0.28	5.9
Cr/Zn-Z5@S1	163.5	0.22	5.5
Cr/Zn-Zn/Z5@S1	186.7	0.21	4.4
Z5	370.6	0.23	0.58
Zn/Z5	382.1	0.19	0.58
Z5@S1	363.1	0.22	0.58
Zn/Z5@S1	383.3	0.20	0.58

Table 3.3 The acidity properties of Z5 zeolite characterized by NH_3-TPD.

Si/Al ratio	Total amount (mmol/g)	Amount (mmol/g)	
		Weak acid sites	Strong acid sites
20	0.67	0.35	0.32
46	0.36	0.12	0.24
82	0.19	0.10	0.09
750	0.12	0.08	0.04

Table 3.4 The acidity properties of different zeolite components used for hybrid catalysts preparation.

Samples	Total amount (mmol/g)	Amount (mmol/g)	
		Weak acid sites	Strong acid sites
Z5	0.36	0.12	0.24
Zn/Z5	0.27	0.09	0.18
Z5@S1	0.15	0.07	0.08
Zn/Z5@S1	0.09	0.04	0.05

Table 3.5 The one pass PX synthesis from syngas over the simplest hybrid catalyst of Cr/Zn-Z5 with varied Si/Al ratio[a]

Catalysts	Si/Al	Conv. (%)		Selectivity (%)[b]								
		CO	CO_2	C_1	C_2-C_5	C_6	C_7	C_8	OX	MX	PX	PX/X
Cr/Zn-Z5	20	62.8	-57.2	9.0	65.8	0.3	14.0	4.9	3.0	0	3.0	50.0
	46	61.0	-48.0	2.4	41.4	4.3	10.0	25.2	6.1	0.1	10.5	62.9
	82	58.0	-46.5	9.3	58	1.9	2.9	12.2	5.8	0.1	9.8	62.4
	750	53.8	-46.7	8.3	32	5.7	7.3	32.3	5.3	0.5	8.6	59.2

[a] Reaction conditions: 5.0 MPa, 673 K, W/F=20.7 $g{\cdot}h{\cdot}mol^{-1}$, 4 h, 0.5 g catalyst, Cr/Zn=2/1, the weight ratio of Cr/Zn to Z5 was 2, syngas $H_2/CO/CO_2/Ar$=62.78/29.3/4.95/2.97. [b] C_2-C_5 including paraffins and olefins, ortho-xylene=OX, meta-xylene=MX, para-xylene=PX, C_6-C_8 are the aromatics except for xylene, PX/X: the ratio of PX to all xylene.

Table 3.6 The catalytic performance of varied catalysts for the one-pass PX synthesis from syngas[a]

Catalysts	Conv. (%)		Selectivity (%)[b]										
	CO	CO_2	MeOH	DME	CH_4	C_2-C_5	C_6	C_7	C_8	OX	MX	PX	PX/X
Cr/Zn	27.5	-27.5	15.9	38.2	30.4	14.0	1.1	0.4	0	0	0	0	0
Cr/Zn-Z5	61.0	-61.0	0	0	2.4	41.4	4.3	10.0	25.2	6.1	0.1	10.5	62.9
Cr/Zn-Z5@S1	55.2	-55.2	0	0	2.4	44.5	6.8	6.8	21.3	4.9	0.3	13.0	71.4
Cr/Zn-Zn/Z5	66.4	-66.4	0	0	3.2	38.5	2.4	9.6	29.7	3.9	0.3	12.4	74.7
Cr/Zn-Zn/Z5@S1 hybrid	55.0	-55.0	0	0	4.4	33.6	3.6	9.5	13.2	8.1	0	27.6	77.3
Cr/Zn+Zn/Z5@S1 dual-layer	34.5	8.0	0.2	0.1	26.8	59.1	8.3	1.2	1.5	0.7	0	2.1	75.0
Cr/Zn+Zn/Z5@S1 granule mixture	50.4	-29.8	0.1	0	7.2	66.6	14.8	3.2	1.2	1.7	0	5.2	75.4

[a] Reaction conditions: 5.0 MPa, 673 K, W/F=20.7 $g \cdot h \cdot mol^{-1}$, 4 h, 0.5 g catalyst, Cr/Zn=2/1, the weight ratio of Cr/Zn to zeolite was 2, syngas $H_2/CO/CO_2/Ar$=62.78/29.3/4.95/2.97. [b] C_2-C_5 including paraffins and olefins, ortho-xylene=OX, meta-xylene=MX, para-xylene=PX, C_6-C_8 are the aromatics except for xylene, PX/X: the ratio of PX to all xylene.

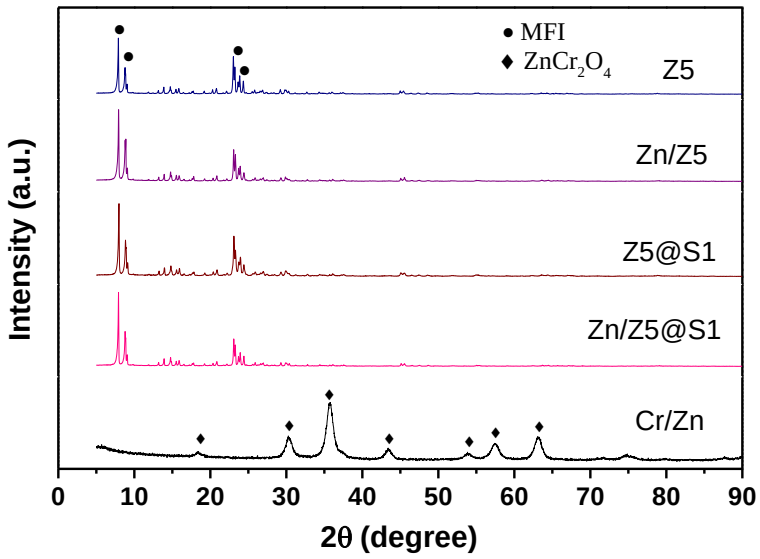

Figure 3.1 XRD patterns of the Z5, Zn/Z5, Z5@S1, Zn/Z5@S1 and Cr/Zn catalysts.

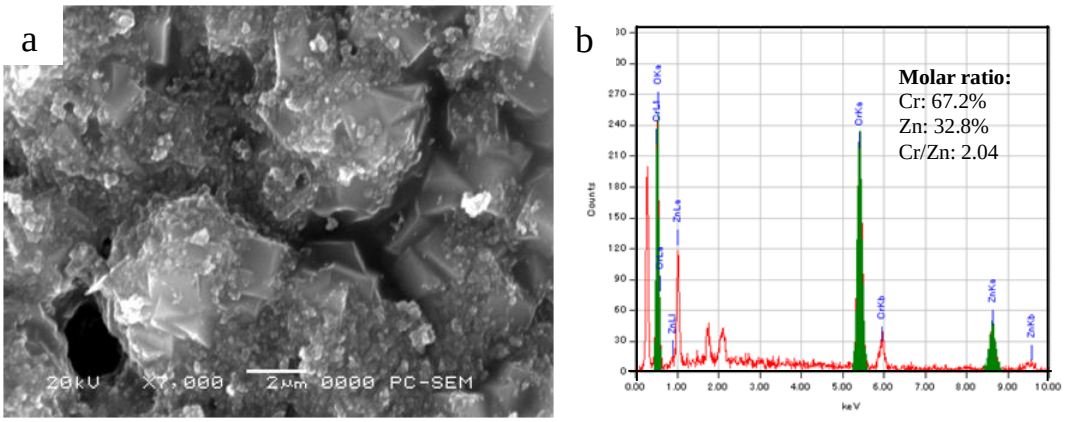

Figure 3.2 The (a) SEM image and (b) EDS analysis results of the Cr/Zn catalyst.

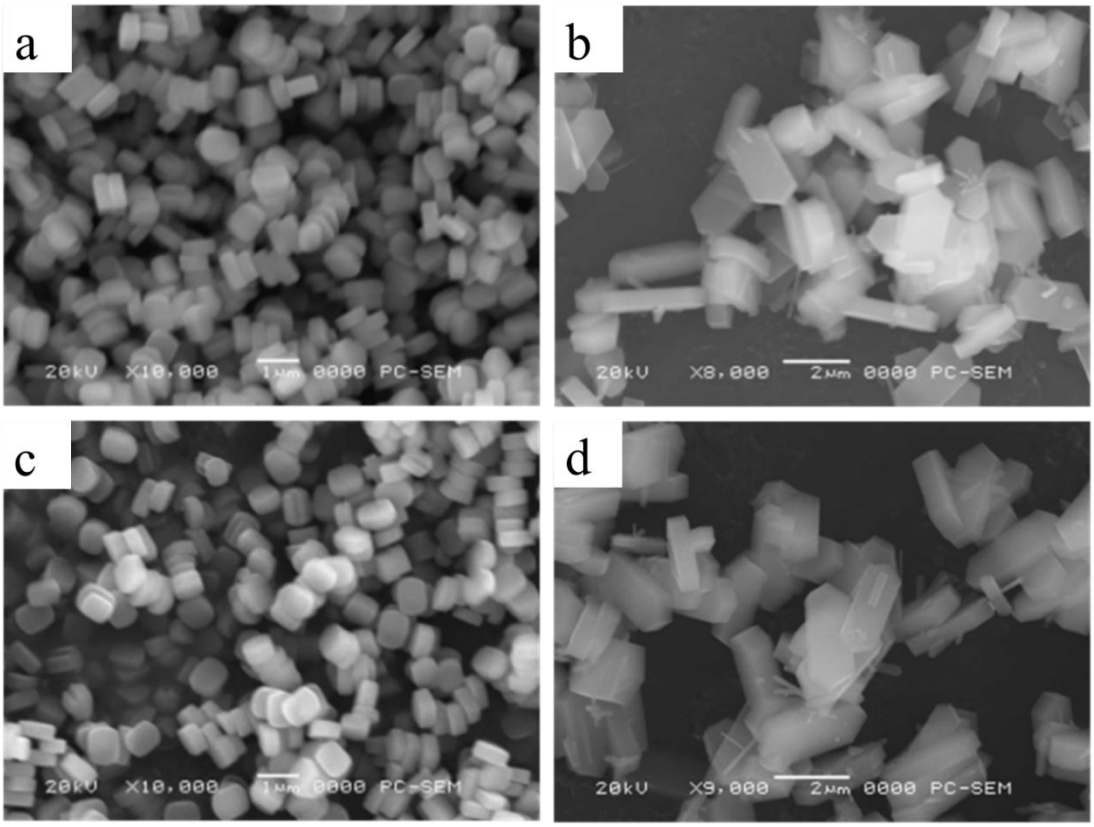

Figure 3.3 SEM images of a) Z5, b) Z5@S1, c) Zn/Z5 and d) Zn/Z5@S1 materials.

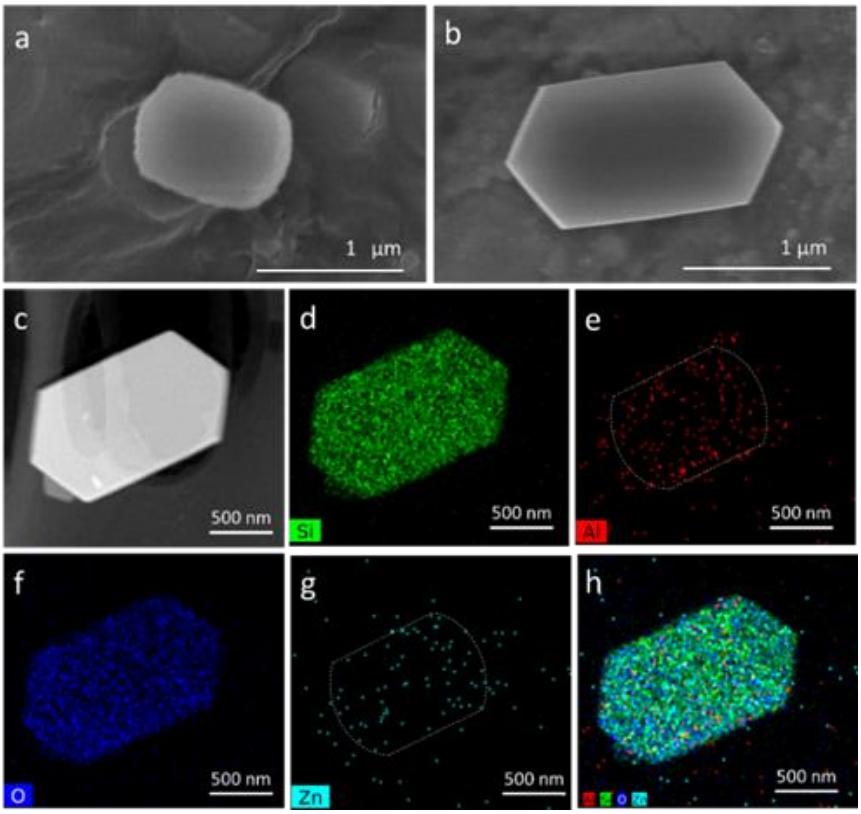

Figure 3.4 The FE-SEM images of (a) Zn/Z5 and (b) the core-shell-structured Zn/Z5@S1 zeolite components; (c) the STEM image of Zn/Z5@S1 zeolite component and the corresponding STEM EDS mapping of (d) Si, (e) Al, (f) O, (g) Zn and (h) the combined Si, Al, O and Zn.

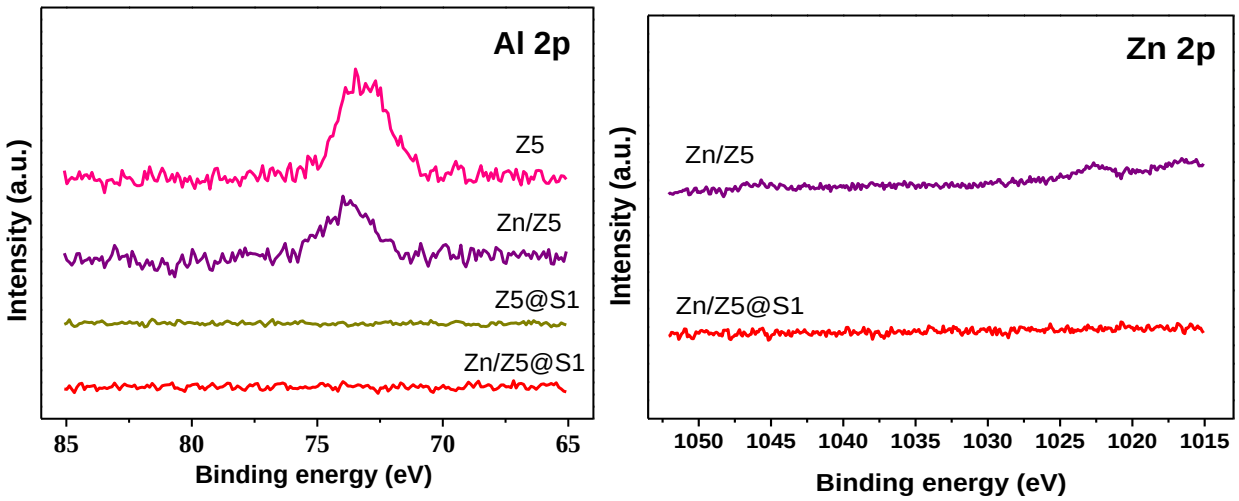

Figure 3.5 The XPS curves of Al and Zn on the zeolite components Z5, Zn/Z5, Z5@S1 and Zn/Z5@S1.

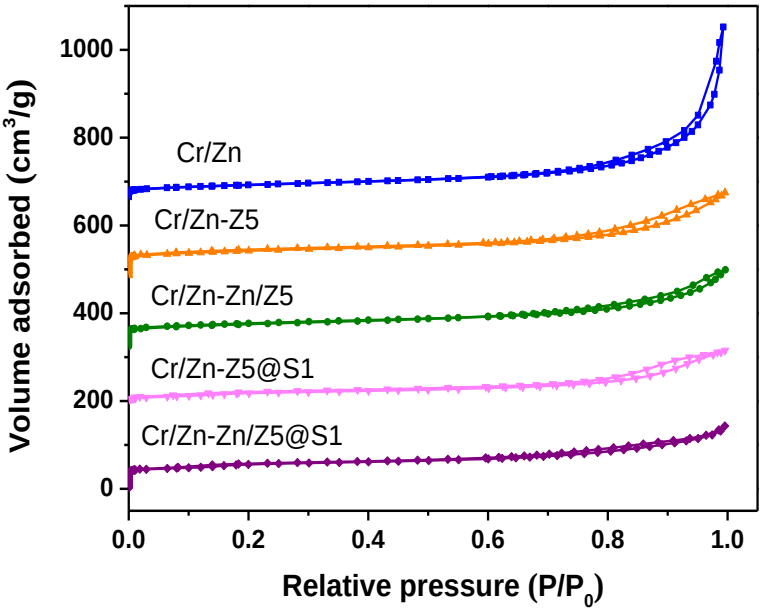

Figure 3.6 The N_2 adsorption-desorption isotherms of Cr/Zn, Cr/Zn-Z5, Cr/Zn-Zn/Z5, Cr/Zn-Z5@S1 and Cr/Zn-Zn/Z5@S1 catalysts.

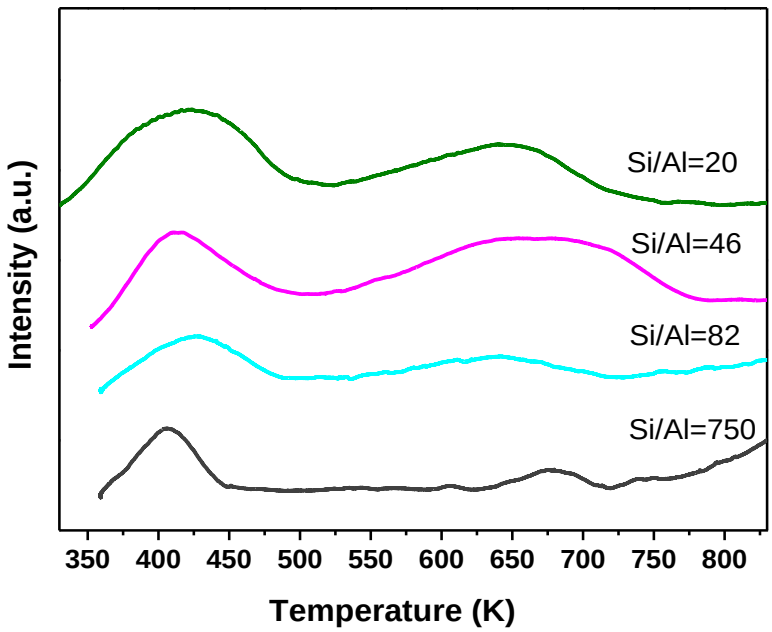

Figure 3.7 The NH_3-TPD curves of Z5 zeolite with different Si/Al ratio of 20, 46, 82 and 750.

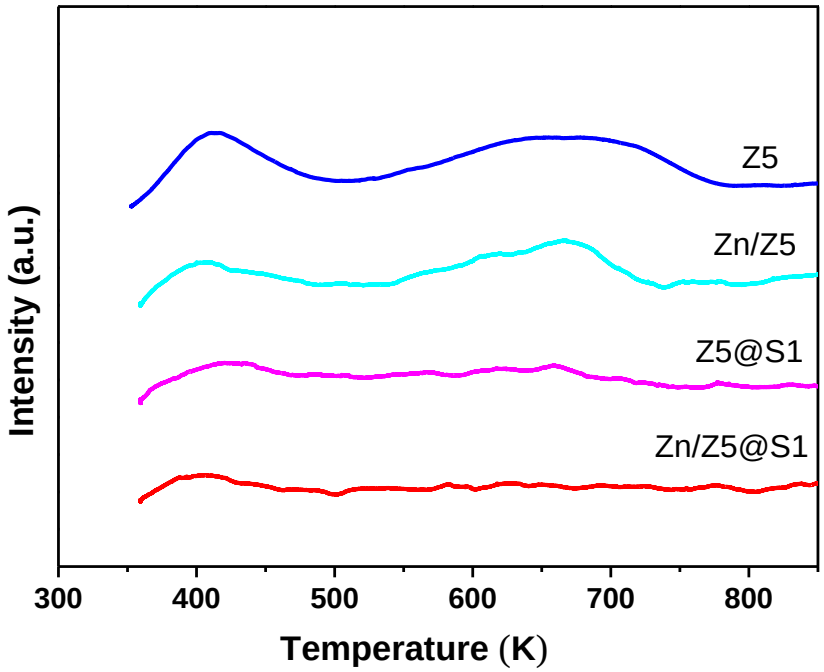

Figure 3.8 The NH_3-TPD curves of Z5, Zn/Z5, Z5@S1 and Zn/Z5@S1.

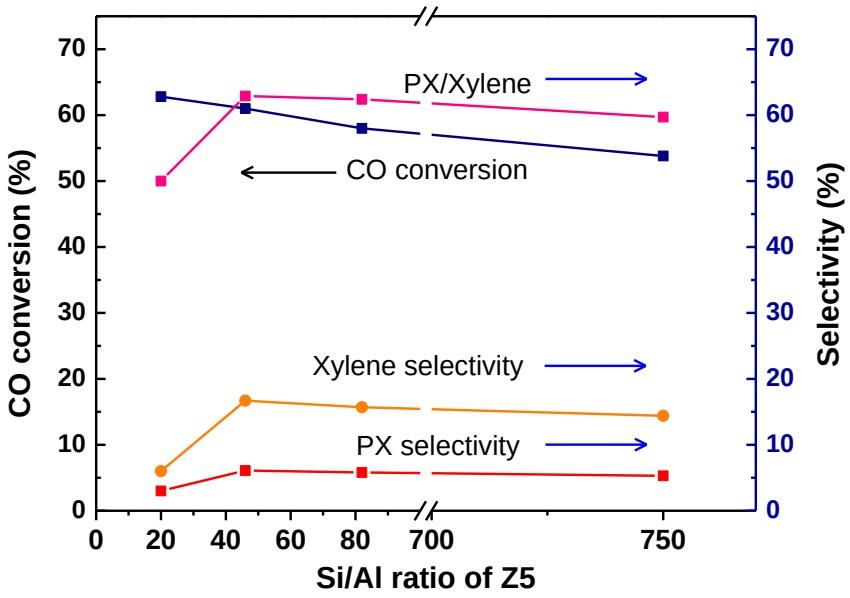

Figure 3.9 The effect varied Si/Al ratio of Z5 in the simplest hybrid catalyst Cr/Zn-Z5 for the one-pass selective conversion of syngas to PX. Reaction conditions: 5.0 MPa, 673 K, W/F=20.7 $g \cdot h \cdot mol^{-1}$, 4 h, 0.5 g catalyst, Cr/Zn=2/1, the weight ratio of Cr/Zn to H-ZSM-5 was 2, syngas $H_2/CO/CO_2/Ar$=62.78/29.3/4.95/2.97.

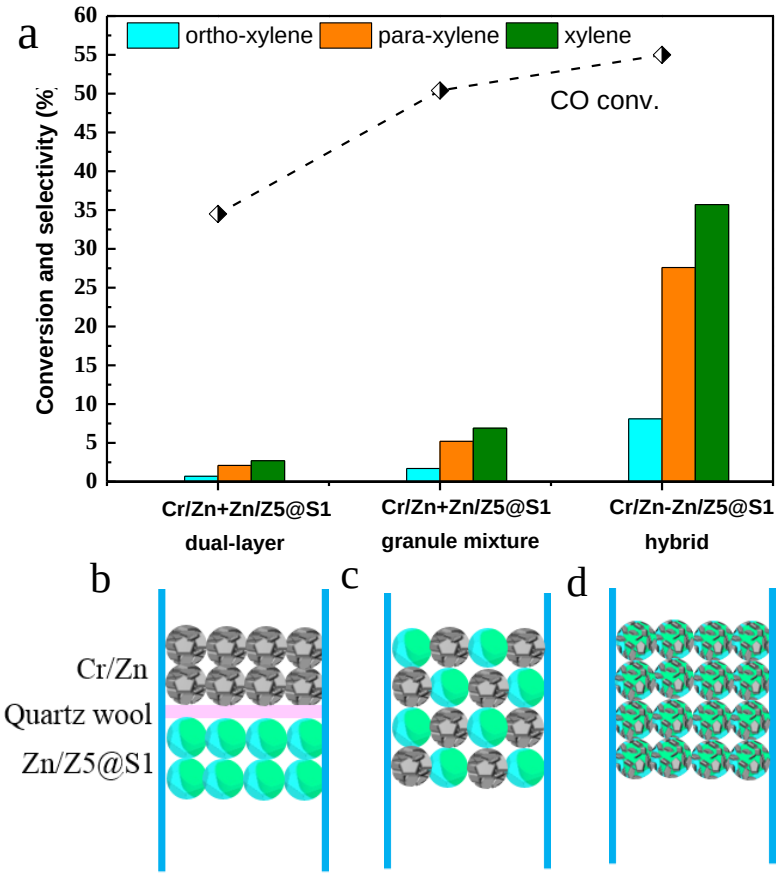

Figure 3.10 The effect of varied assembly models of two active components on the catalytic performance in reaction. Reaction conditions: 5.0 MPa, 673 K, W/F=20.7 $g \cdot h \cdot mol^{-1}$, 4 h, 0.5 g catalyst, Cr/Zn=2/1, the weight ratio of Cr/Zn to Zn/Z5@S1 was 2, syngas $H_2/CO/CO_2/Ar$=62.78/29.3/4.95/2.97.

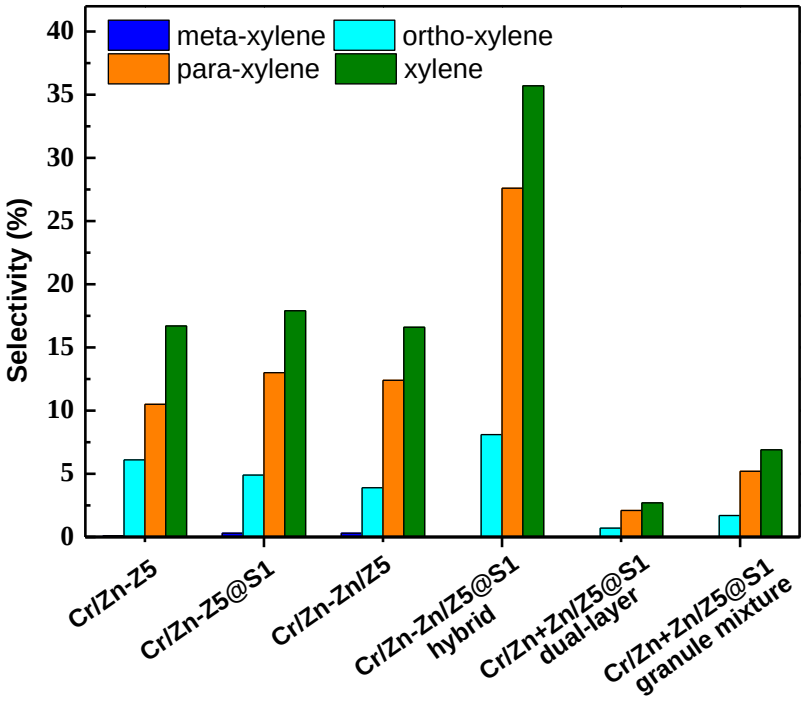

Figure 3.11 The distribution of total xylene and isomers (OX, MX and PX) over varied hybrid catalysts. Reaction conditions: 5.0 MPa, 673 K, W/F=20.7 $g \cdot h \cdot mol^{-1}$, 4 h, 0.5 g catalyst, Cr/Zn=2/1, the weight ratio of Cr/Zn to zeolite was 2, syngas $H_2/CO/CO_2/Ar$=62.78/29.3/4.95/2.97.

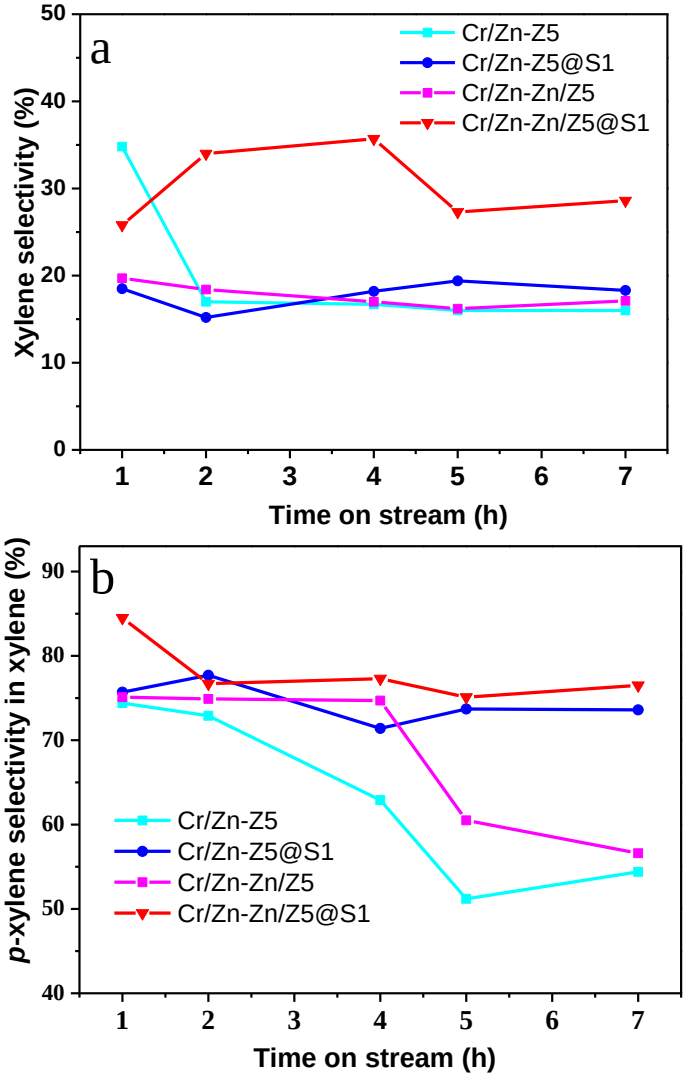

Figure 3.12 The xylene selectivity (a) and the p-xylene selectivity in the total xylene isomers (b) as a function of time on stream. Reaction conditions: 5.0 MPa, 673 K, W/F=20.7 $g \cdot h \cdot mol^{-1}$, 0.5 g catalyst, Cr/Zn=2/1, the weight ratio of Cr/Zn to zeolite was 2, syngas $H_2/CO/CO_2/Ar$=62.78/29.3/4.95/2.97.

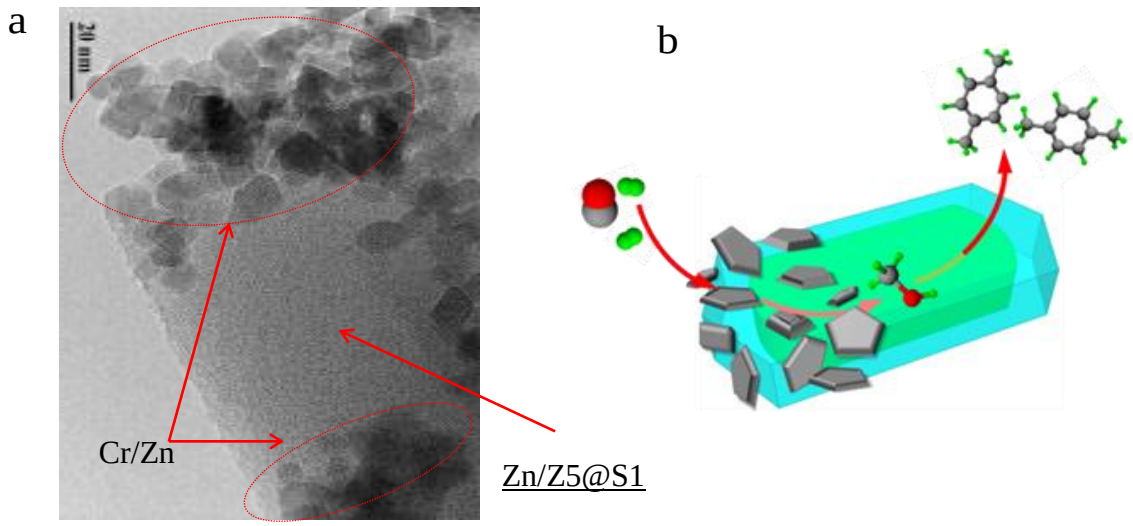

Figure 3.13 (a) the TEM image of the Cr/Zn-Zn/Z5@S1 hybrid catalyst (b) the reaction mechanism of the one-pass selective syngas conversion to para-xylene over the hybrid catalyst Cr/Zn-Zn/Z5@S1.

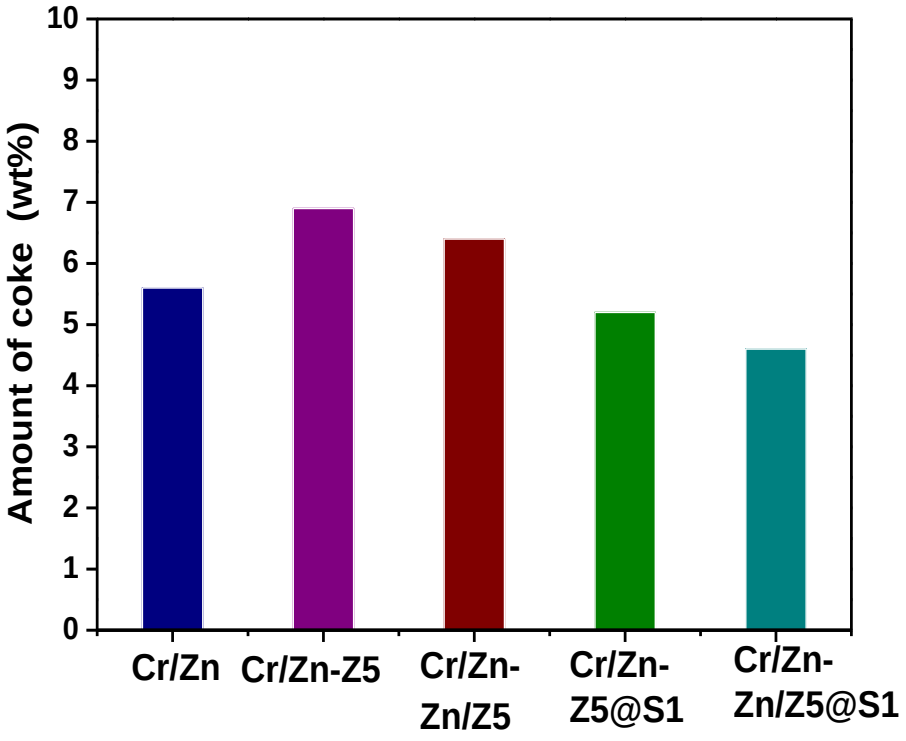

Figure 3.14 The coke deposition amount on the spent hybrid catalysts measured by TG.

Chapter 4

Summary

With the increasing depletion of crude oil and global environmental concerns, the development and utilization of renewable energy into useful chemicals have received considerable attention all over the world. Biomass is a kind of renewable source of energy, which can make us less dependent on fossil fuels. Moreover, syngas is a vital junction point that bridges the non-petroleum carbon resources and other basic chemicals, which can be produced from biomass, coal and nature gas. Therefore, efficiently employing and converting of renewable resources to alternative flues and chemicals is considered as an effective route in current science research field.

The designing of catalysts is one of vital factors to affect the catalytic performance and product distribution in catalytic route. In this thesis, we successfully designed and synthesized three types of high performance of catalysts with special structure, and various reaction systems were employed to test their catalytic activity. The Ni/ZrO_2-SiO_2-B bimodal pore catalyst was prepared for enhanced hydrogen production by steam reforming of vegetable oil; the Pd/SiO_2-SZ zeolite capsule catalyst was designed for direct synthesis LPG from syngas; and the Cr/Zn-Zn/Z5@S1 hybrid catalyst with Zn/Z5@S1 core-shell structure zeolite was synthesized for one-pass conversion of syngas to para-xylene. The catalytic performance and selectivity of target products are greatly enhanced with these new design and preparation of catalysts.

As mentioned in Chapter 1, a bimodal ZrO_2-SiO_2-B support was successfully synthesized by introducing ZrO_2 sol precursors inside pores of a commercial silica gel Q-30 followed by calcination. While a unimodal ZrO_2-SiO_2-U support was obtained when using $ZrO(NO_3)_2 \cdot 2H_2O$ as the precursor. The characterization results illustrated that the bimodal ZrO_2-SiO_2-B support showing increased BET surface area was beneficial for the dispersion of Ni species. Among all catalyst studied bimodal

Ni/ZrO_2-SiO_2-B catalyst exhibited highest oil conversion and H_2 formation rate. These results were inferred that the improved Ni dispersion, enhanced Ni-support interaction, as well as facilitated diffusion of reactant and products from bimodal structure, and promotional effect of ZrO_2 contributed to the superior catalytic performance of bimodal catalyst.

As mentioned in Chapter 2, a Pd/SiO_2-SZ zeolite capsule catalyst was prepared by a developed dual-layer growth method. The catalyst characterization demonstrated that the Pd/SiO_2-SZ zeolite capsule catalyst had millimeter-sized core-shell structure with a compact H-ZSM-5 shell. Pd/SiO_2-SZ zeolite capsule catalyst was used to investigate the catalytic performance of direct LPG synthesis from syngas. The LPG selectivity on this Pd/SiO_2-SZ zeolite capsule catalyst reaches 34.4% with CO conversion of 14.1%. The unexpected superior performance of Pd/SiO_2-SZ zeolite capsule catalyst is ascribed to the tailor-made core-shell-like structure, which provides a confined reaction environment for LPG direct synthesis from syngas.

As mentioned in Chapter 3, we presented a successful hybrid catalyst Cr/Zn-Zn/Z5@S1 for one-pass conversion of syngas to para-xylene with high activity, selectivity, stability and lower CO_2 formation. The selectivity of PX obtained by this hybrid catalyst reached up to 77.3% in the xylene isomers and accounted for 27.6% of the total hydrocarbons products at the CO conversion of 55.0%. This hybrid catalyst contained two components: one was Cr/Zn and the other one was a core-shell-structured Zn/Z5@S1 zeolite. The combination of two components in this hybrid catalyst performed a well-organized tandem catalysis process, syngas to methanol and methanol to PX exclusively. The special core-shell structure of Zn/Z5@S1 could effectively seal the exposed active sites of zeolite, by which to depress the formation of unwanted xylene isomers and promote the oriented synthesis of PX.

The new findings in this thesis are beneficial to designing and building nano catalysts with special structure for high-value-added chemicals synthesis from

non-petroleum source (biomass or syngas). The presented catalysts preparation method in this thesis can be also extended to other catalysis processes.

List of publications

1. **Peipei Zhang**, Li Tan, Guohui Yang, Noritatsu Tsubaki. One-pass selective conversion of syngas to para-xylene. ***Chemical Science***, 2017, 8, 7941-7946. IF=8.667

2. **Peipei Zhang**, Guohui Yang, Li Tan, Peipei Ai, Ruiqin Yang, Noritatsu Tsubaki. Direct synthesis of liquefied petroleum gas from syngas over H-ZSM-5 enwrapped Pd-based zeolite capsule catalyst. ***Catalysis Today***, 2018, 303, 77-85. IF=4.26

3. Kai Tao, Hiroyuki Arano, **Peipei Zhang**, Peipei Ai, Lei Han, Noritatsu Tsubaki. Enhanced hydrogen production from steam reforming of vegetable oil over bimodal ZrO_2-SiO_2 supported Ni catalyst. ***Chemistry Select***, 2017, 2, 527-532.

4. **Peipei Zhang**, Yibo Hu, Baihai Li, Qiuju Zhang, Chen Zhou, Hongbo Yu, Xuejun Zhang, Liang Chen, Bryan Eichhorn, and Shenghu Zhou. Kinetically stabilized Pd@Pt core-shell octahedral nanoparticles with thin Pt layers for enhanced catalytic hydrogenation performance. ***ACS Catalysis***, 2015, 5 (2), 1335-1343. IF=10.614

5. Xuejun Zhang, **Peipei Zhang**, Hongbo Yu, Zhen Ma, Shenghu Zhou. Mesoporous KIT-6 Supported Pd-MxOy (M=Ni, Co, Fe) Catalysts with Enhanced Selectivity for p-chloronitrobenzene Hydrogenation. ***Catalysis Letters***, 2015, 145, 3, 784-793. IF=2.799

6. Qinhong Wei, Guohui Yang, Xinhua Gao, Li Tan, Peipei Ai, **Peipei Zhang**, Peng Lu, Yoshiharu Yoneyama, Noritatsu Tsubaki. A facile ethanol fuel synthesis from dimethyl ether and syngas over tandem combination of Cu-doped HZSM35 with Cu-Zn-Al catalyst. ***Chemical Engineering Journal***, 2017, 316, 832-841. IF=5.310

7. Pengfei Zhu, Guohui Yang, Jian Sun, Ronggang Fan, **Peipei Zhang**, Yoshiharu Yoneyama, Noritatsu Tsubaki. A hollow Mo/HZSM-5 zeolite capsule catalyst: preparation and enhanced catalytic properties in methane dehydroaromatization. ***Journal of Materials Chemistry A***, 2017. 5, 8599-8607. IF=8.867

8. Noriyuki Yamane, Yang Wang, Jie Li, Yingluo He, **Peipei Zhang**, Letrunghieu Nguyen, Li Tan, Peipei Ai, Xiaobo Peng, Ye Wang, Guohui Yang, Noritatsu Tsubaki. Building premium secondary reaction field with a miniaturized capsule

catalyst to realize efficient synthesis of liquid fuel directly from syngas. ***Catalysis Science &Technology***, 2017, 7, 1996-2000. IF=5.287

9. Qinhong Wei, Guohui Yang, Xinhua Gao, Noriyuki Yamane, **Peipei Zhang**, Guoguo Liu, Noritatsu Tsubaki. Ni/Silicalite-1 coating being coated on SiC foam: A tailor-made monolith catalyst for syngas production using a combined methane reforming process. ***Chemical Engineering Journal***, 2017, 327, 465-473. IF=5.310

10. Pengfei Zhu, Jian Sun, Guohui Yang, Guoguo Liu, **Peipei Zhang**, Yoshiharu Yoneyama, Noritatsu Tsubaki. Tandem catalytic synthesis of benzene from CO_2 and H_2. ***Catalysis Science &Technology***, 2017, 7, 2695-2699. IF=5.287

11. Minghui Tan, Yuki Ishikuro, Yuta Hosoi, Noriyuki Yamane, Peipei Ai, **Peipei Zhang**, Guohui Yang, Mingbo Wu, Ruiqin Yang, Noritatsu Tsubaki. PPh_3 functionalized Rh/rGO catalyst for heterogeneous hydroformylation: Bifunctional reduction of graphene oxide by organic ligand. ***Chemical Engineering Journal***, 2017, 330, 863-869. IF=5.310

12. Chuang Xing, Peipei Ai, **Peipei Zhang**, Xinhua Gao, Ruiqin Yang, Noriyuki Yamane, Jian Sun, Prasert Reubroycharoen, Noritatsu Tsubaki. Fischer-Tropsch synthesis on impregnated cobalt-based catalysts: New insights into the effect of impregnation solutions and pH value. ***Journal of Energy Chemistry***, 2016, 25, 994-1000. IF=2.322

13. Huan Liu, Kai Tao, **Peipei Zhang**, Wei Xu and Shenghu Zhou. Enhanced catalytic performance for metathesis reactions over order tungsten and aluminum co-doped mesoporous KIT-6 catalysts. ***New Journal of Chemistry***, 2015, 39, 7971-7978. IF=3.269

List of Conferences

1. Direct synthesis of liquefied petroleum gas from syngas over H-ZSM-5 enwrapped Pd-based zeolite capsule catalyst. 16th Korea-Japan Symposium on Catalysis, Hokkaido, Japan, May 15-17, 2017. **Oral.**
2. Kinetically stabilized Pd@Pt core-shell octahedral nanoparticles with thin Pt layers for enhanced catalytic hydrogenation performance. 116th Catalysis Society of Japan, Mie, Japan, September 16-18, 2015. **Oral.**
3. Mesoporous KIT-6 supported Pd-MxOy (M=Ni, Co, Fe) catalysts with enhanced selectivity for p-chloronitrobenzene hydrogenation. The 17th National Conference on Catalysis of China, Hangzhou, China, October 13-17, 2014. Poster.

Acknowledgements

Undertaking this PhD has been a truly life-changing experience for me and it would not have been possible to do without the support and guidance that I received from many people throughout my doctoral period.

I would like to express my heartfelt gratitude to my supervisor, Professor Noritatsu Tsubaki, for his warm-heart encouragement and most valuable advice, especially for giving me an opportunity to study in Japan for doctor degree. What is more important is that his profound erudition and rigorous attitude to science influenced me deeply, inspiring me to move towards the scientific way of passing the future. Without his pushing me ahead, encouragement and guidance, I could not have completed this paper.

My sincere thanks also go to Associate Professor Yoshiharu Yoneyama for providing me with advice and assistance in the experiment. I shall extend my thanks to Dr. Guohui Yang, for his invaluable advice, constant encouragement and precise modification, and I admire his knowledge and his personality. His keen and vigorous academic observation enlightens me not only in my doctor academic career but also in my future study.

I would like to give my deeply thanks to senior sister apprentice and senior brother apprentice of Tsubaki lab for offering me a lot of help in my experiment and life. They are Dr. Kai Tao, Mr. Li Tan, Dr. Chuang Xing, Dr. Jian Sun, Dr. Peng Lu, Dr. Xiaobo Peng, Dr. Qinhong Wei, Dr. Minghui Tan, Dr. Pengfei Zhu, Dr. Jie Li, Dr. Xinhua Gao, Dr. Peipei Ai, Mr. Guoguo Liu, Mr. Yang Wang, Mr. Xiaobo Feng, Mr. Yingluo He, Ms. Yuan Fang, Mr. Xiaoyu Guo, Mr. Yu Cui, Mr. Hangjie Li, Mr. Lisheng Guo. Besides, I also want to thanks Dr. Chunhui Luan, Dr. Ye Tian, Dr. Fanzhi Meng, Ms. Thachapan Atchimarungsri, Mr. Yuichi Suzuki, Mrs. Hitomi Itou, Mr. Mitsunori Masaki, Prof. Shigehiro Kagaya, Prof. Akira Taguchi, Ms. Farihin Nur, Mr. Masato Omi and many other Japanese teachers and students in university of Toyama for their assistance in

study and life.

Last but not least, I would like to express my thanks to my beloved family and my friends for their continued encouragement and spiritual support during my study.